iScience

Article

NKG2D-CAR-targeted iPSC-derived MSCs efficiently target solid tumors expressing NKG2D ligand

Graphical abstract

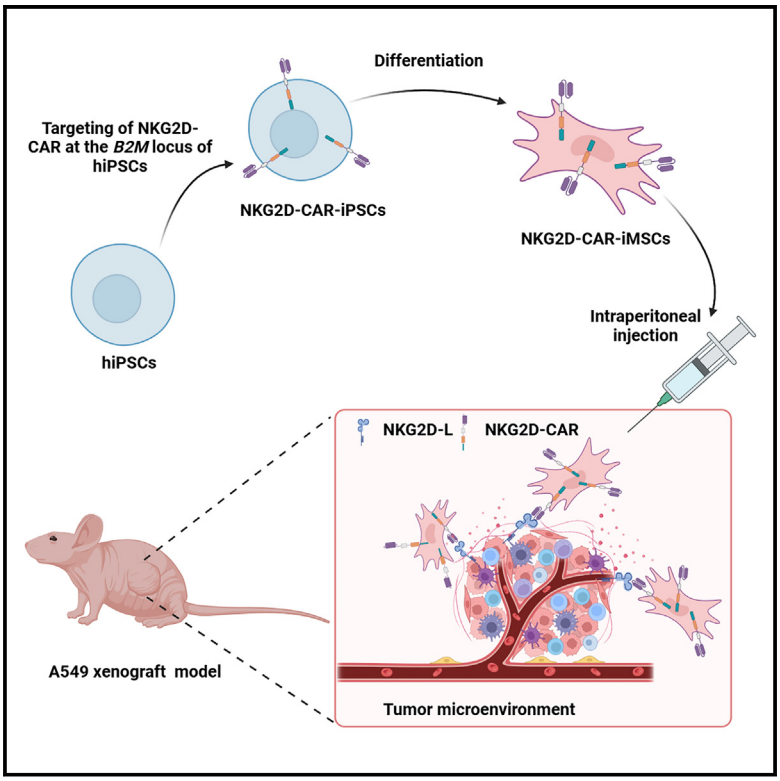

Highlights

- Efficient expression of targeted NKG2D-CAR at *B2M* locus in iPSC-derived MSCs
- Enhanced binding of NKG2D-CAR-iMSCs to tumor cells expressing NKG2D-L *in vitro*
- Upregulation of genes related to cell adhesion and migration in NKG2D-CAR-iMSCs
- Enhanced targeting specificity of NKG2D-CAR-iMSCs to tumor cells in mouse model

Authors

Shuqing Tang, Yusang Zhang, Peiyun Wang, ..., Qian Hu, Mai Feng, Desheng Liang

Correspondence

liangdesheng@sklmg.edu.cn

In brief

Natural sciences; Biological sciences; Molecular biology; Cell biology; Systems biology; Cancer systems biology; Cancer

Tang et al., 2025, iScience *28*, 112343
May 16, 2025
https://doi.org/10.1016/j.isci.2025.112343

CellPress

iScience

CellPress
OPEN ACCESS

Article

NKG2D-CAR-targeted iPSC-derived MSCs efficiently target solid tumors expressing NKG2D ligand

Shuqing Tang,[1,3] Yusang Zhang,[1,3] Peiyun Wang,[1] Qiyu Tang,[1] Yating Liu,[1] Fan Lu,[1] Mengting Han,[1] Miaojin Zhou,[1] Qian Hu,[1] Mai Feng,[2] and Desheng Liang[1,4,*]

[1]Center for Medical Genetics & Hunan Key Laboratory of Medical Genetics, School of Life Sciences, Central South University, Changsha 410078, China

[2]Hunan Key Laboratory of Animal Models for Human Diseases, School of Life Sciences, Central South University, Changsha 410078, China

[3]These authors contributed equally

[4]Lead contact

*Correspondence: liangdesheng@sklmg.edu.cn

https://doi.org/10.1016/j.isci.2025.112343

SUMMARY

Mesenchymal stem cells (MSCs) hold potential in cancer therapy; however, insufficient tumor homing ability and heterogeneity limit their therapeutic benefits. Obviously, the homogeneous induced pluripotent stem cell (iPSC)-derived mesenchymal stem cells (iMSCs) with enhanced ability of tumor targeting could be the solution. In this study, a CAR containing the NKG2D extracellular domain was targeted at the *B2M* locus of iPSCs to generate NKG2D-CAR-iPSCs, which were subsequently differentiated into NKG2D-CAR-iMSCs. *In vitro*, NKG2D-CAR significantly enhanced migration and adhesion of iMSCs to a variety of solid tumor cells expressing NKG2D ligands. RNA sequencing (RNA-seq) revealed significant upregulation of genes related to cell adhesion, migration, and binding in NKG2D-CAR-iMSCs. In A549 xenograft model, NKG2D-CAR-iMSCs demonstrated a 57% improvement in tumor-homing ability compared with iMSCs. In conclusion, our findings demonstrate enhanced targeting specificity of NKG2D-CAR-iMSCs to tumor cells expressing NKG2D ligands *in vitro* and *in vivo*, facilitating future investigation of iMSCs as an off-the-shelf living carrier for targeted delivery of anti-tumor agents.

INTRODUCTION

Preclinical and clinical cancer research increasingly highlights the therapeutic potential of cell-based strategies. Genetically engineered mesenchymal stem cells (MSCs) exhibiting tumor tropism are now frequently utilized in both regenerative medicine and oncology.[1,2] Human induced pluripotent stem cell (hiPSC)-derived MSCs (iMSCs) surpass tissue-derived MSCs in terms of homogeneity, quality consistency, and *in vitro* expansion potential,[3] and it was confirmed that iMSCs closely mimic tissue-derived MSCs in morphology, immunophenotype, multilineage differentiation, and tumor-targeting ability.[4] However, the limited tumor-targeting efficacy of MSCs hinders broader clinical application.[5] Enhancing MSC tumor targeting for precision drug delivery is thus one of the critical research priorities.

The chimeric antigen receptor (CAR) technology is a potent tool for endowing immune cells with specific targeting ability. NKG2D, a receptor whose ligands are broadly expressed in solid tumors, such as ovarian, cervical cancer, lung cancer et al., but minimally in normal cells, emerges as an exceptionally promising target.[6–8] The NKG2D receptor is a member of the NK-activated receptor family, and its ligand (NKG2D-L) consists of two families in human, including MICA, MICB, and ULBP1-6.[7] NKG2D expression on immune cells, such as natural killer (NK) and T cells, enhances their proliferation, cytotoxicity, and cytokine release upon binding to NKG2D-L on malignant cells, thereby augmenting antitumor responses.[9] To date, NKG2D-CAR, comprising an artificial transmembrane and intracellular signaling domain, has primarily been applied in T and NK cells to bolster tumor targeting and antitumor effects, demonstrating the potent antitumor activity of the NKG2D/NKG2D-L axis.[10] Yet, CAR-T and CAR-NK cell therapies confront challenges like cell dysfunction, cytokine release syndrome, tumor microenvironment (TME)-induced immunosuppression, and poor tumor infiltration.[11–13] MSCs are recognized for their innate immune-modulating functions and their ability to penetrate the TME effectively,[14] suggesting that MSCs are ideal carriers for NKG2D-CAR with promising prospects for precise drug delivery to tumor sites and immunomodulation.

Theoretical considerations suggest that NKG2D-CAR expression on MSCs could enhance their tumor-targeting ability, thereby facilitating the precise release of therapeutic drugs. Evidence supports that CAR technology can improve MSC tumor targeting,[15,16] but traditional MSCs derived from tissues raised several disadvantages, such as limited ability of proliferation and heterogeneity arising from different donors or different tissues[17]; meanwhile, engineered MSCs with viral vectors introduce heterogeneity and safety risks.[18]

In this study, we engineered induced pluripotent stem cells (iPSCs) derived from a healthy donor by integrating a CAR

structure, featuring the extracellular domain of NKG2D, into the widely accepted safe harbor *B2M* locus using the CRISPR/Cas9 system. The *B2M* gene encodes β2-microglobulin, which is the beta (light) chain of human leukocyte antigen class I (HLA-I). Multiple studies have demonstrated that insertion at *B2M* site does not affect normal cellular functions but rather helps to reduce immunogenicity.[19–21] This approach circumvents the safety hazards associated with viral gene-editing methods, facilitating the generation of NKG2D-CAR-iPSCs that were then differentiated into NKG2D-CAR-iMSCs. This research provides pioneering evidence of the augmented tumor-targeting ability of NKG2D-CAR-iMSCs in both cellular and organismal models, thus laying the groundwork for future studies on the utilization of NKG2D-CAR-iMSCs as a reliable, homogeneous living carrier system for the precise delivery of antitumor therapeutics.

RESULTS

Engineered iPSCs express NKG2D with targeted integration of NKG2D-CAR at the *B2M* locus

The targeting vector B2M-NKG2D-CAR (Figure 1A) was engineered to achieve site-specific expression of NKG2D-CAR at the *B2M* locus of B6-iPSCs, which were reprogrammed from exfoliated renal tubular epithelial cells (urine cells) of a healthy male donor by our laboratory.[22] We utilized primers B2M-up-F/R and B2M-down-F/R (Table S1) for PCR identification, and the results confirmed the successful integration of the construct, yielding PCR products of 1,091 bp and 1,117 bp, respectively (Figure 1B). Sanger sequencing of these products revealed a precise alignment with the expected sequence, thereby confirming the successful targeting of exogenous genes (Figure 1C). Quantitative reverse transcription polymerase chain reaction (RT-qPCR) was employed to assess NKG2D-CAR transcript levels, which were significantly elevated in NKG2D-CAR iPSCs compared to B6-iPSCs (Figure 1D; Table S1). Flow cytometry analysis was conducted to evaluate the surface expression of NKG2D on NKG2D-CAR iPSCs, confirming successful NKG2D expression (Figure 1E). Given that our target cleavage site is located on exon 1 of the *B2M* locus, we utilized flow cytometry to assess β2-microglobulin expression and found it to be normal, suggesting that our target gene was integrated as a single copy (Figures 1F and 1G). Notably, the genetically modified iPSC clones maintained a normal morphology (Figure 1H), displayed normal karyotypes, and exhibited no detectable off-target mutations (Figure S1; Table S1).

Generation and characterization of iMSCs derived from NKG2D-CAR-iPSCs and B6-iPSCs

Using the STEMdiff mesenchymal progenitor kit, we differentiated iPSCs into iMSCs (Figure 2A). The iMSCs derived from NKG2D-CAR-iPSCs exhibited a typical spindle-shaped morphology and a vortex distribution (Figure 2B). Consistent with previous reports, all iMSC strains were positive for CD90, CD73, CD44, and CD105 but negative for CD45, CD34, and HLA-DR (Figure 2C). RT-qPCR results showed that NKG2D maintained a high level of expression in iMSCs (Figure 2D), and flow cytometry confirmed this, revealing that NKG2D-CAR-iMSCs highly expressed NKG2D on the cell surface, which was clearly different from B6-iMSCs (Figure 2E). Since β2-microglobulin is the beta (light) chain of HLA-I, its function is crucial for maintaining HLA-I surface expression. We examined HLA-I expression on iMSCs and confirmed that the single-copy integration of NKG2D-CAR at the *B2M* locus did not disrupt β2-microglobulin function (Figure 2E). Notably, NKG2D-CAR expression was not achieved at alternative safe harbor sites, such as rDNA and *AAVS1* (Figure 2F), even with successful targeting (Figure S2). This suggested that the *B2M* site is an ideal locus for efficient expression. Consequently, we obtained iMSCs capable of stably expressing NKG2D, with higher homogeneity and reproducibility than adult stem cells.

NKG2D-CAR functionalization improves the iMSCs adhesion to NKG2D-L-expressing tumor cells

To assess the enhanced interaction between NKG2D-CAR-iMSCs and tumor cells expressing NKG2D-L (Figure S3), we conducted cell interaction experiments as previously described (Figure 3A).[15] The binding strength between iMSCs and tumor cells was quantified by comparing the percentage of double-positive cells across different groups. We systematically varied the ratios of iMSCs to tumor cells (2:1, 1:1, 1:2) to determine the optimal conditions for adhesion. Our results demonstrated a significant improvement in the adhesion ability of NKG2D-CAR-iMSCs to various solid tumors compared to B6-iMSCs ($p < 0.05$). Notably, NKG2D-CAR-iMSCs exhibited a 50% increase in adhesion to A549 cells ($p < 0.001$), and this enhancement was proportional to the increasing ratio of A549 to iMSCs (Figures 3B and 3C). Similar trends were observed in MCF7 cells, with a significant increase in adhesion ($p < 0.01$). In contrast, no significant differences were detected with Hep3B2.1-7 cells, which do not express NKG2D-L[23] (Figure S4), suggesting a specific interaction between NKG2D-CAR-iMSCs and NKG2D-L-expressing tumors. Collectively, these findings indicate that NKG2D-CAR effectively enhances the adhesion of iMSCs to a broad spectrum of solid tumors, highlighting its potential in targeted cancer therapy. In addition to the 1.5h time point, we established experimental groups at 2, 4, and 6 h to investigate the potential time-dependent effects of the adherence between iMSCs and tumor cells (Figure S5). Overall, the results presented that the adhesion of NKG2D-CAR-iMSCs to tumor cells exhibited an optimal duration, beyond which the adhesion efficiency did not increase with extended time.

NKG2D-CAR-iMSCs display enhanced migration toward NKG2D-L-expressing tumor cells

To dissect the influence of NKG2D signaling on iMSCs migration, we executed a series of Transwell migration assays, as presented in Figure 4A. In the negative control group devoid of tumor cells in the lower chamber, we demonstrated that there was no significant difference in the baseline migration between the B6-iMSCs and NKG2D-CAR-iMSCs (Figures S6A and S6B). Our initial investigations utilized A375 cells and revealed that NKG2D-CAR-iMSCs exhibited a significantly enhanced migratory response toward A375 cells, with a migration rate 3.5-fold higher than that of B6-iMSCs ($p < 0.0001$), as detailed in Figures 4B and 4C. This experiment was then replicated with H1299, A549, and MCF7 tumor cells. Consistent with our

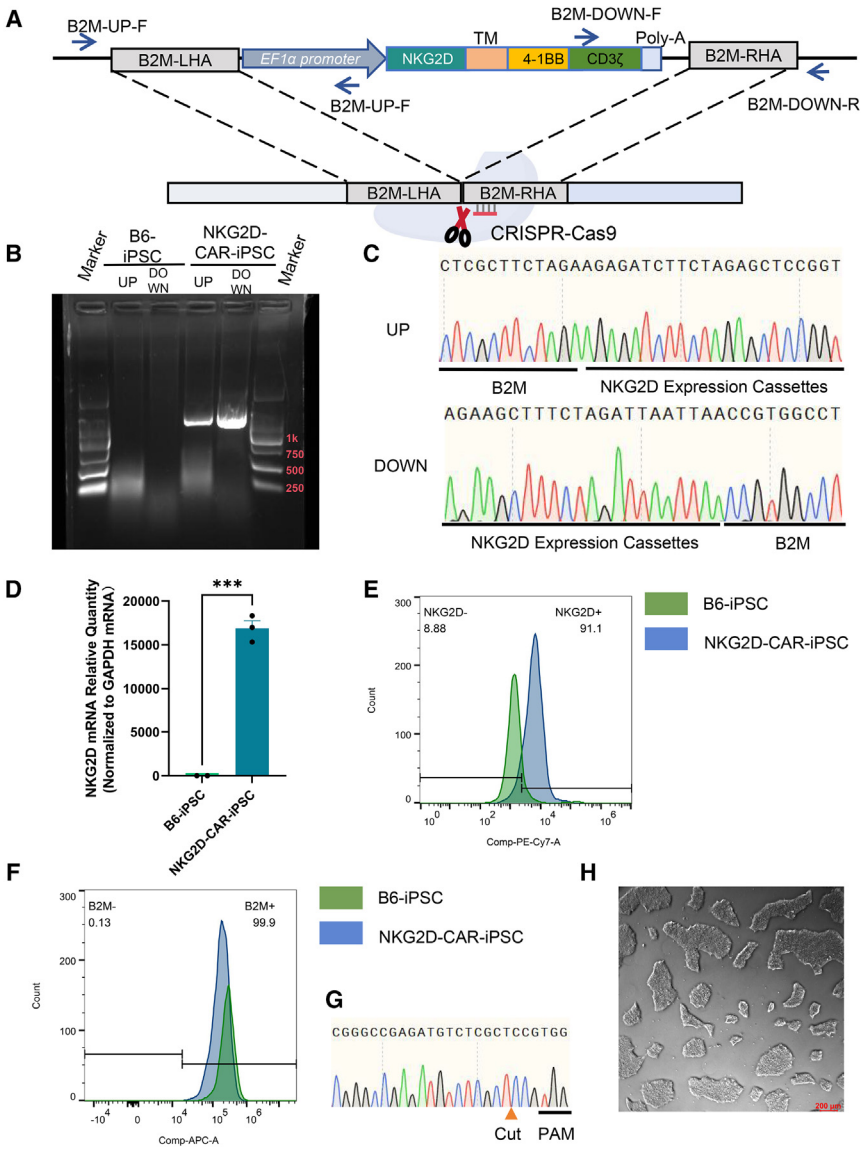

Figure 1. Engineered iPSCs express NKG2D with targeted integration of NKG2D-CAR at the *B2M* locus

(A) Schematic diagram of *B2M* targeting vector B2M-NKG2D-CAR and gene targeting process flowcharts. Binding sites of primers B2M-up-F/R and B2M-down-F/R that were utilized to identify site-specifically integrated clones are indicated.

(B) Gel electropherogram for PCR identification. B6-iPSCs, iPSCs from a healthy donor.

(C) Sanger sequencing results of PCR products spanning the upstream and downstream homology arms.

(D) Quantitative RT-PCR analysis of NKG2D mRNA transcription levels in NKG2D-CAR-iPSCs compared to B6-iPSCs. (Data are mean ± SEM; $n = 3$; $^{***}p < 0.001$, determined by Student's two-tailed t test.)

(E) Flow cytometric analysis for the surface expression of NKG2D in iPSCs. The horizontal axis shows signal intensity of PE-Cy7-NKG2D.

(F) Flow cytometric analysis for the surface expression of β2-microglobulin in iPSCs. The horizontal axis shows signal intensity of APC-B2M.

(G) Sanger sequencing results of the NKG2D-CAR-iPSCs of *B2M* locus.

(H) Morphology of representative NKG2D-CAR-iPSCs (scale bar: 200 μm).

findings in A375 cells, NKG2D-CAR-iMSCs showed a significant increase in migration, with a range of 1- to 2-fold higher compared to B6-iMSCs ($p < 0.05$ for all comparisons), as illustrated in Figures 4B and 4C. These results suggest that NKG2D signaling plays a pivotal role in the interaction between iMSCs and tumors, augmenting not only the adhesion of iMSCs to tumor cells but also their migratory ability.

RNA-seq revealed a significant upregulation of the genes related to cell adhesion, migration, and binding in NKG2D-CAR-iMSC

To confirm whether there are other factors involved in interacting between NKG2D-CAR-iMSCs and tumor cells, we performed RNA-seq. Compared to B6-iMSCs, we identified 678 genes that were significantly upregulated ($p < 0.05$) and 528 genes downregulated ($p < 0.05$) (Figure 5A). These differentially expressed genes underwent Gene Ontology (GO) enrichment analysis, revealing significant associations with binding and alterations in cell membrane and extracellular matrix components, including terms related to membrane, membrane part ($p < 0.05$) (Figure 5B). These findings suggest that NKG2D overexpression modulates the cell membrane and extracellular matrix of iMSCs, thereby enhancing their targeting ability. Volcano plot analysis identified several upregulated genes implicated in cell adhesion and migration, such as fibulin-2 (*FBLN2*), C-type lectin domain family 14 member A (*CLEC14A*), cadherin EGF LAG seven-pass G-type receptor 1 (*CELSR1*), leucine-rich repeat-containing protein 15 (*LRRC15*), and laminin subunit alpha-2 (*LAMA2*), along with genes related to cell membranes and the extracellular matrix, such as Thy-1 cell surface antigen (*THY1*) and sulfatase 2 (*SULF2*) (Figure 5C). The clustering heatmap clearly delineated the distinct expression profiles between NKG2D-CAR-iMSCs and B6-iMSCs (Figure 5D). Subsequent RT-qPCR validation confirmed the significant upregulation of *CADM1*, *LAMA2*, *FBLN2*, *CELSR1*, *CLEC14A*, and *LRRC15* in NKG2D-CAR-iMSCs ($p < 0.05$) (Figure 5E) (please check Table S1 for sequences of the primers of genes mentioned above). Collectively, these results demonstrate that NKG2D-CAR expression induces substantial alterations in the cell membrane, extracellular matrix, and adhesive properties of iMSCs, which may have significant implications for their targeting ability. It is worth noting that the downstream molecules associated with the intracellular domain of our CAR, including

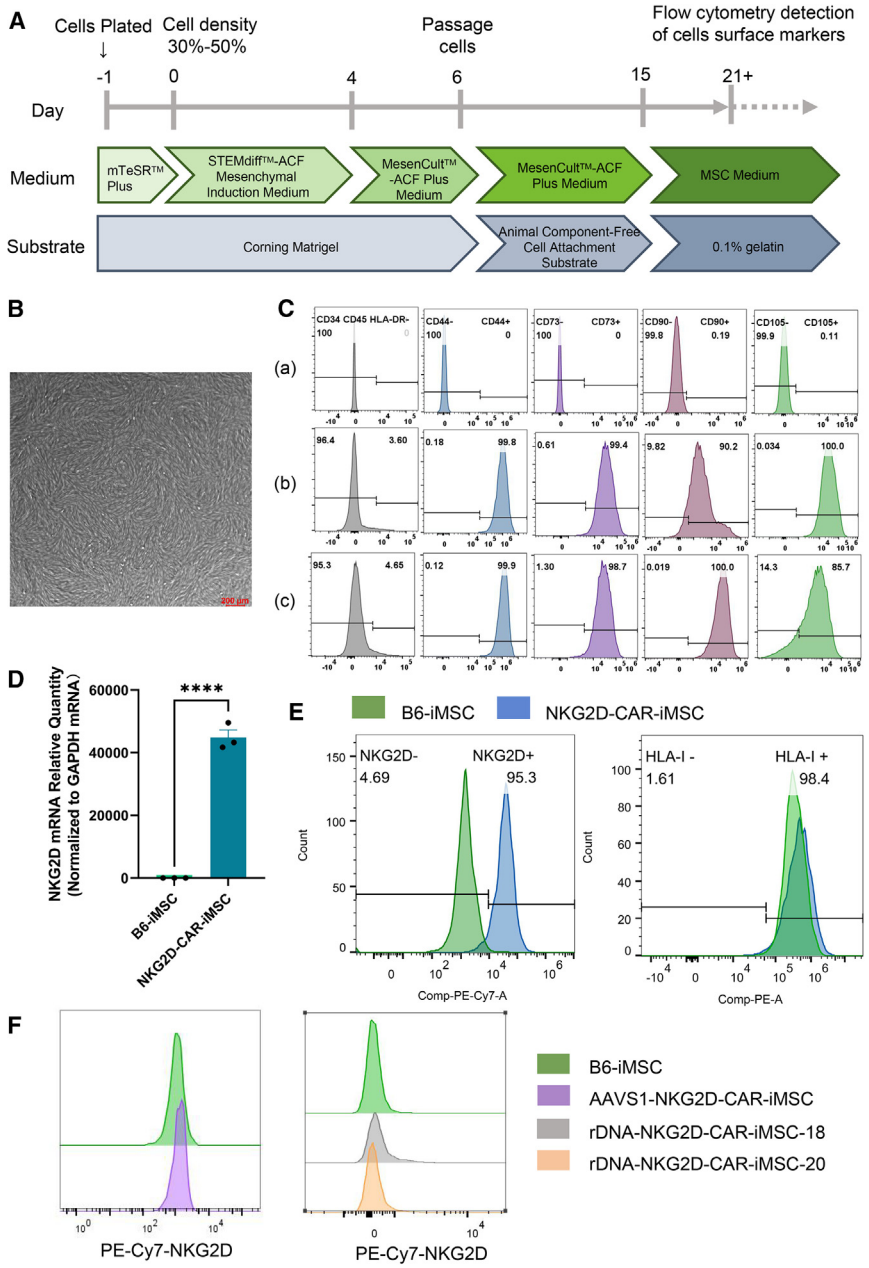

Figure 2. Generation and characterization of iMSCs

(A) Flowcharts of iMSCs differentiation procedure.

(B) Morphology of the iMSCs derived from NKG2D-CAR-iPSCs (scale bar: 200 μm).

(C) Flow cytometric analysis for detection of B6-iMSCs and NKG2D-CAR-iMSCs surface markers CD34, CD45, HLA-DR, CD44, CD73, CD90, and CD105. a, blank control; b, B6-iMSCs; c, NKG2D-CAR-iMSCs.

(D) Quantitative RT-PCR analysis of NKG2D mRNA transcription levels in NKG2D-CAR-iMSCs and B6-iMSCs. (Data are mean ± SEM; $n = 3$; ****$p < 0.0001$ determined by Student's two-tailed t test).

(E) Flow cytometric analysis for the surface expression of NKG2D and HLA-I in iMSCs. The horizontal axis shows signal intensity of PE-Cy7-NKG2D and PE-HLA-I.

(F) Flow cytometric analysis for the surface expression of NKG2D in rDNA-NKG2D-iMSCs and AAVS1-NKG2D-iMSCs. The horizontal axis shows signal intensity of PE-Cy7-NKG2D.

4-1BB and CD3-ζ, such as Zeta-chain-associated protein kinase 70 (*ZAP70*), nuclear factor of activated T cells 5 *(NFAT5*), and tumor necrosis factor (TNF)-receptor-associated factor 2 (*TRAF2*) were not activated in NKG2D-CAR-iMSCs (Figure S7A). Notably, *ZAP70*, the ζ-chain-associated protein kinase 70 that is directly related to CD3-ζ, exhibited very low or undetectable expression levels in both MSCs and NKG2D-CAR-iMSCs. Therefore, we propose that the current signaling changes in NKG2D-CAR-iMSCs are not due to the signal transduction of the CAR intracellular domain but are more likely influenced by the engineering process of iMSCs themselves. Additionally, we observed that genes associated with angiogenesis were downregulated in NKG2D-CAR-iMSCs through RNA-seq data, which suggests that although NKG2D-CAR enhances the adhesion and migration of iMSCs to tumor cells, it also reduces the risk of promoting tumor angiogenesis (Figure S7B).

NKG2D-CAR engineering enhances the pro-inflammatory phenotype of iMSCs and promotes tumor cell apoptosis *in vitro*

To investigate the impact of NKG2D-CAR-iMSCs on immune cell function and their subsequent tumor-killing efficacy, we conducted co-culture experiments involving iMSCs, A549 tumor cells, and peripheral blood mononuclear cells (PBMCs). The experimental results demonstrated that NKG2D-CAR-iMSCs significantly increased the apoptosis rate of A549 cells induced by PBMCs compared with B6-iMSCs, and the total apoptosis rate was elevated by nearly 50% (Figures 6A and 6B). By comparing the RNA-seq data, we observed that relative to B6-iMSCs, the expression levels of several pro-inflammatory cytokines, such as, interleukin-33 (IL-33), IL-18, IL-12 were significantly upregulated in NKG2D-CAR-iMSCs. In contrast, immunosuppressive cytokines, with the exception of a slight upregulation of transforming growth factor β (TGF-β), exhibited downregulation, including IL-6, IL-10, and prostaglandin-endoperoxide synthase 2 *(*PTGS2), and nearly undetectable expression of indoleamine 2,3-dioxygenase 1 (IDO1) (Figure 6C). These findings are consistent with the co-culture results, suggesting that NKG2D-CAR enhances the pro-inflammatory phenotype of iMSCs.

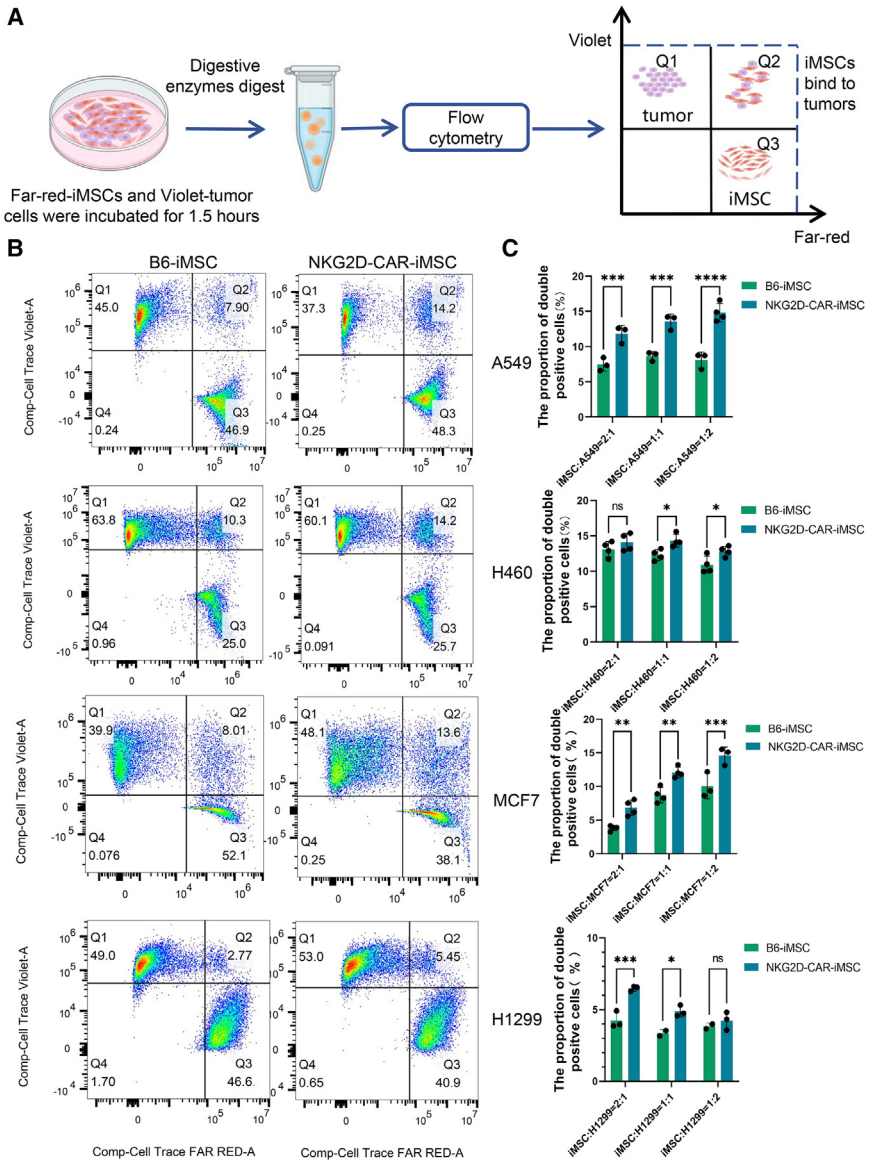

Figure 3. Detection of iMSCs adherence ability

(A–C) (A) Schematic representation of cell interaction experiments, classifying cells into four clusters: Q1 (tumor cells alone), Q2 (iMSCs and tumor cells bound), and Q3 (iMSCs alone) (B and C) Representative flow cytometry plots of iMSCs interaction with A549, H460, MCF7, and H1299 at a 1:1 ratio (B). And statistics of percentage of double-positive cells at a 2:1, 1:1, and 1:2 ratio (C). See also Figures S4 and S5. (Data are mean ± SEM; n = 2–4; $*p < 0.05$, $**p < 0\ 0.01$, $***p < 0.001$, $****p < 0.0001$, as determined by one-way ANOVA).

Subsequently, we employed flow cytometry to analyze the proliferation, activation, and exhaustion of T cells within the co-culture system. We observed that both B6-iMSCs and NKG2D-CAR-iMSCs increased the proportion of $CD4^+$ T cells (Figure 6D) and regulatory T cells (Tregs) (Figure 6E), consistent with previous literature reports.[24–27] However, we also noted a significant upregulation of the T cell activation marker CD69 in both B6-iMSCs and NKG2D-CAR-iMSCs (Figure 6F), which was consistent with our previous findings,[28] as well as a modest increase in the proliferation marker Ki67, although the latter did not reach statistical significance (Figure 6G). Notably, compared with B6-iMSCs, NKG2D-CAR-iMSCs enhanced the proportion of $CD8^+CD25^+$ cells, which is associated with $CD8^+$ T cell activation (Figure 6H). Meanwhile, no significant changes were observed in the cytotoxicity markers Granzyme B (GZMB) and CD107a (LAMP-1) of $CD8^+$ T cells (Figure S8), indicating that NKG2D-CAR-iMSCs did not impair the cytotoxic function of $CD8^+$ T cells. The upregulation of the early exhaustion marker programmed death-1 (PD-1) and the downregulation of the late exhaustion marker T cell immunoglobulin and mucin-domain containing-3 (TIM-3) suggest a complex effect of iMSCs on T cells in the *in vitro* co-culture system; no significant differences were observed between NKG2D-CAR-iMSCs and B6-iMSCs in these aspects (Figure S8).

Integrating the results of tumor cell apoptosis and RNA-seq data, our findings demonstrate that, compared with B6-iMSCs, the expression of multiple pro-inflammatory cytokines is upregulated in NKG2D-CAR-iMSCs, which is conducive to immune activation and enhances the cytotoxicity of immune cells against tumor cells. These characteristics provide further assurance for NKG2D-CAR-iMSCs to serve as an effective vehicle for the delivery of anti-tumor factors.

NKG2D-CAR improves iMSCs targeting and retention in the tumor in A549 xenograft model

To assess the targeting ability of NKG2D-CAR-iMSCs to tumors, we validated their efficacy following intraperitoneal injection in an A549 xenograft model in nude mice (Figure 7A). Dorsal imaging revealed that NKG2D-CAR-iMSCs exhibited the highest signal intensity at the tumor site, whereas B6-iMSCs were more broadly distributed throughout the body (Figure 7B). Subsequent analysis of signals from various organs and the tumor indicated that NKG2D-CAR-iMSCs displayed a notably enhanced tumor signal, which was only surpassed by the signal intensity in the liver and was higher than that observed in the heart, kidney, lung, and spleen (Figure 7C). In contrast, the tumor signal from B6-iMSCs was comparable to that of the spleen and obviously lower than the liver signal. To quantify tumor targeting, we calculated the ratio of tumor site signal to liver signal, demonstrating

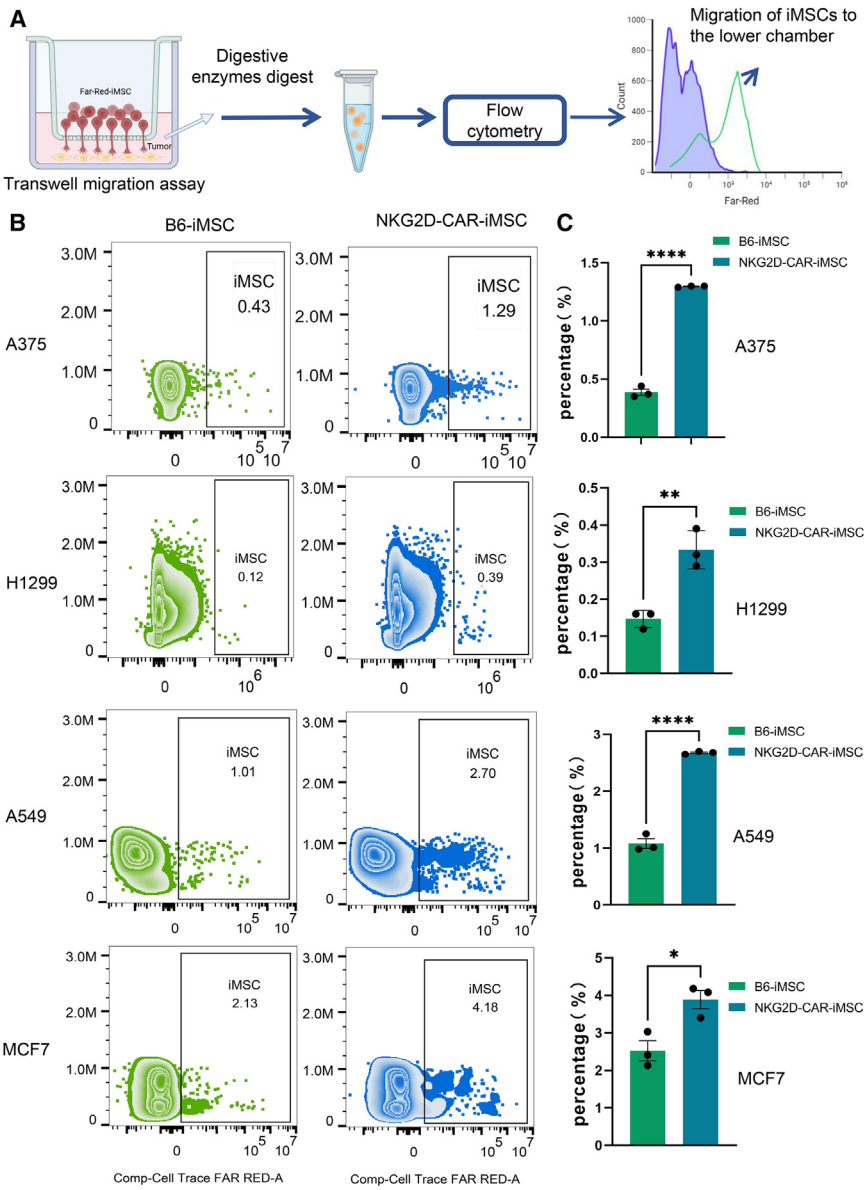

Figure 4. IMSC migration assays in the Transwell system

(A) Schematic representation of cell migration experiment flowchart.

(B and C) Representative flow cytometry plots of far-red (iMSCs) signaling in underlying A375, H1299, A549, and MCF7 cells (B) and statistics of percentage of that (C).

(Data are mean ± SEM; $n = 3$; $^{*}p < 0.05$, $^{**}p < 0.01$, $^{****}p < 0.0001$ as determined by Student's two-tailed t test). See also Figure S6.

that NKG2D-CAR-iMSCs had a significantly higher tumor targeting ability than B6-iMSCs ($p < 0.05$, Figure 7D). We also compared the fluorescence signal intensities in the spleen, lung, and kidney relative to the liver, and no significant differences were observed between the NKG2D-CAR-iMSC group and the B6-iMSC group (Figures S9A and S9C). Additionally, we compared intraperitoneal and tail vein injections, finding that the former was more effective for iMSCs to reach the tumor site, with NKG2D-CAR-iMSCs showing eight times higher signal intensity at the tumor site after intraperitoneal injection compared to tail vein injection ($p < 0.001$, Figures7E, 7F, and S10). Although NKG2D-CAR-iMSCs targeted the tumor site with greater efficacy, they did not directly kill the tumor, as tumor volume measurements remained unchanged (Figure 7G). Throughout the experiment, mouse body weight remained stable, and no significant differences were observed between experimental groups, indicating a favorable safety profile for NKG2D-CAR-iMSCs (Figure 7G). Additionally, biochemical analysis of serum revealed no significant abnormalities in biochemical markers associated with liver or kidney function; all values were within the normal reference range (Figure S11). Histological examination of hematoxylin and eosin (H&E)-stained sections of the liver, lung, spleen, and kidney also showed no overt pathological changes in these organs (Figure S12). These findings further demonstrate the safety of NKG2D-CAR-iMSCs.

DISCUSSION

In this study, we engineered iPSCs with high expression of NKG2D-CAR by targeting the expression cassette at the *B2M* locus. These cells successfully differentiated into iMSCs that met the established MSC criteria and stably expressed NKG2D. We found that elevated NKG2D levels significantly enhanced iMSCs adhesion and migration to tumor cells expressing NKG2D-L. In the A549 xenograft mouse model, NKG2D-CAR-iMSCs showed enhanced tumor-targeting ability over controls. These results suggest that NKG2D-CAR-iMSCs, with their enhanced tumor tropism, high proliferation activity, and consistent quality, may serve as a versatile therapeutic tool for immune modulation in tumor or inflammatory environments.

NKG2D is an activating immune receptor that plays a significant role in anti-tumor immunity. The ligands for NKG2D are typically expressed on cancerous or stressed cells and are generally not present in healthy tissues, which makes it a promising candidate for CAR therapy. NKG2D-CAR-T and CAR-NK cells are extensively studied for their potential in cancer treatment. However, they face challenges such as cytokine release syndrome, limited efficacy against solid tumors, and immunosuppression by the TME, which restrict the clinical application potential of the NKG2D target.[29–34] MSCs possess natural

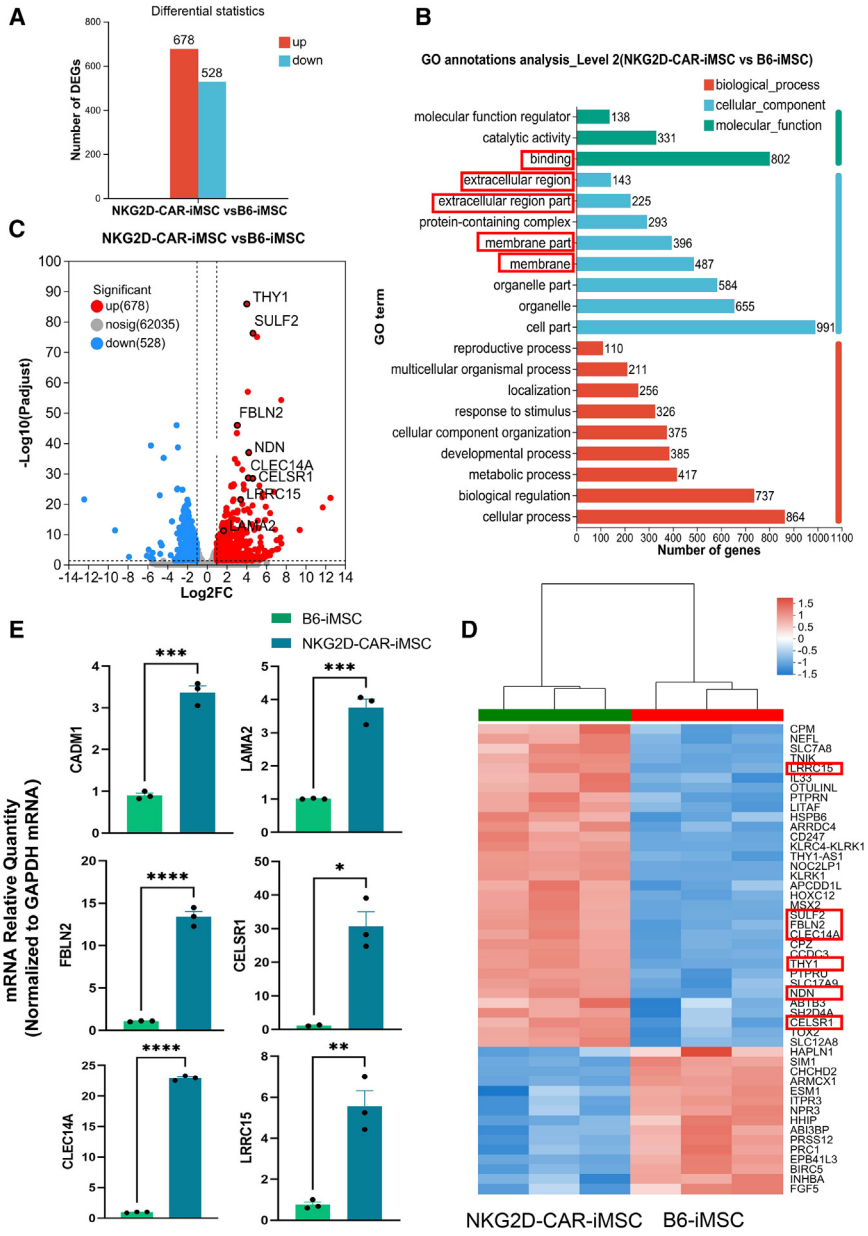

Figure 5. Comparative RNA-seq analysis between B6-iMSCs and NKG2D-CAR-iMSCs

(A) Bar chart of differentially expressed genes (DEGs) in NKG2D-CAR-iMSCs and B6-iMSCs.

(B) Gene ontology (GO) enrichment analyses of DEGs.

(C) Volcano plot illustrating DEGs, with upregulated genes represented by red dots, downregulated genes by blue dots, and genes without significant expression indicated by gray dots.

(D) Heatmap displaying the top 50 DEGs ranked by *p* value, with red indicating high expression and blue indicating low expression.

(E) RT-qPCR validation of DEGs associated with cell adhesion.

(Data are mean ± SEM; $n = 3$; $^{*}p < 0.05$, $^{**}p < 0.01$, $^{***}p < 0.001$, $^{****}p < 0.0001$, as determined by Student's two-tailed *t* test).

immune-modulating functions, can effectively penetrate the TME, and their capacity to carry and secrete a range of therapeutic factors positions them as a promising adjunct to cellular immunotherapy.[2,35–38] Our study showed that NKG2D-CAR modification significantly enhanced the tumor-targeting ability of iMSCs, resulting in a 57% increase in signal intensity within the tumor area. This improvement suggested the therapeutic potential of NKG2D-CAR-iMSCs. In the future, the use of NKG2D-CAR-iMSCs for the delivery of therapeutic factors, such as IL-2 and anti-PD-1 antibodies, will facilitate the preferential accumulation of these agents in the TME, thereby reducing systemic toxicities associated with conventional drug administration. As a targeted delivery vehicle, NKG2D-CAR-iMSCs also hold significant potential in gene-directed enzyme prodrug therapy (GDEPT), such as 5-fluorocytosine activation, which can optimize the delivery and expression of enzyme genes to the tumor site and enhance therapeutic efficacy.

Within the field of CAR-MSC research, a number of studies have reported notable progress. Giulia et al. developed a GD2-tCAR-MSC construct for the delivery of sTRAIL, which showed substantial binding affinity to malignant gliomas with high GD2 expression.[39] In another study, Olivia et al. constructed an EcCAR-MSC targeting E-calmodulin, demonstrating that the CD28ζ domain plays an essential role in enhancing the immunosuppressive properties of MSCs, thus advancing CAR-MSC research.[16] However, these studies relied on tissue-derived MSCs and used lentiviral vectors for genetic engineering, which comes with inherent limitations, including limited proliferative potential, potential immunogenicity of viral vectors, and the inherent heterogeneity of tissue-derived MSCs that can complicate the consistency and predictability of therapeutic outcomes.[17] In our study, we overcame these limitations by employing non-viral methods to edit iPSCs and subsequently differentiating them into iMSCs. These iMSCs displayed enhanced proliferation and stability compared to their tissue-derived MSCs, presenting clear and significant advantages for their clinical application.

RNA-seq data from our study revealed that NKG2D-CAR expression induced significant changes in the cell membrane and extracellular matrix of iMSCs. These modifications potentially enhanced adhesion and migration capabilities, which have improved tumor targeting. However, they also raised concerns regarding the potential for off-target effects. Our *in vitro* and *in vivo* experiments, conducted to address these concerns,

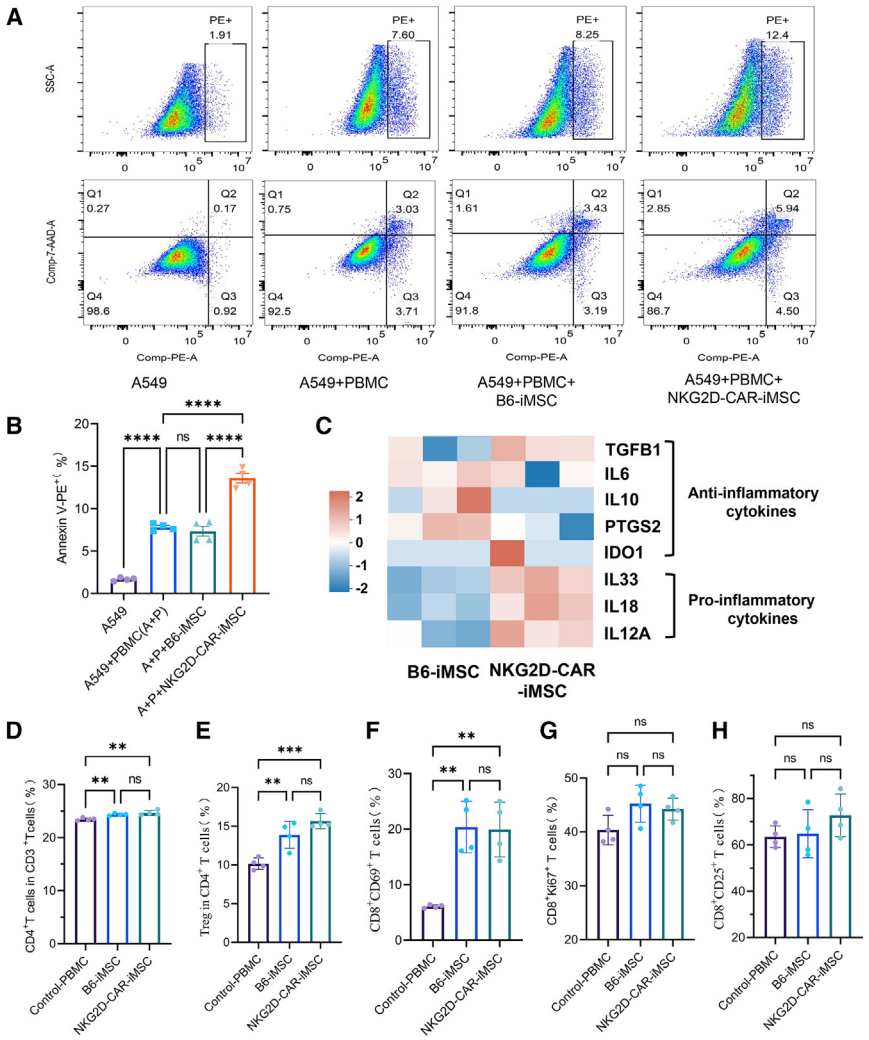

Figure 6. Analysis of iMSCs immune modulation

(A) Flow cytometric analysis of apoptotic A549 stained with Annexin V-PE/7-ADD on various samples.

(B) Quantification of apoptotic A549 cells.

(C) Heatmap showing the expression profiles of immunomodulator genes in B6-iMSC and NKG2D-CAR-iMSC; red indicates high expression, whereas blue indicates low expression.

(D–H) Immune cell subset analysis in PBMCs co-cultured with A549 and iMSCs *in vitro*. (D) Frequency of $CD4^+$ T cells within $CD3^+$ T cells. (E) Frequency of Tregs ($CD4^+$ $CD25^+$ $FoxP3^+$) within $CD4^+$ T cells. (F–H) Frequency of $CD8^+$ T cell subsets ($CD8^+$ $CD69^+$, $CD8^+$ $KI67^+$, $CD8^+$ $CD25^+$) within $CD8^+$ T cells. See also Figure S8.

(Data are mean ± SEM; $n = 4$; $^*p < 0.05$, $^{**}p < 0.01$, $^{***}p < 0.001$, $^{****}p < 0.0001$, as determined by one-way ANOVA).

suggested that this enhanced adhesion was not a universal phenomenon across all cell types. Notably, *in vivo* studies showed that NKG2D-CAR-iMSCs exhibited more robust signaling in tumor tissues compared to other healthy tissues; in non-tumoral regions, only slight increases were observed in the lungs. Although these signal alterations enhance the targeting of NKG2D-CAR-iMSCs to the tumor site, it cannot be denied that they may also increase the complexity of iMSCs functions within the TME. Based on the current experimental results, no significant differences were observed between NKG2D-CAR-iMSCs and iMSCs in their *in vivo* impact on tumor growth, indicating that the effects of these signal changes are within a controllable range. Additionally, the iMSCs used in our study, compared to tissue-derived MSCs, exhibit greater homogeneity and stability,[3,4,40] which facilitates our control over their functions within the TME.

It is noteworthy that the role of iMSCs within the tumor microenvironment is highly complex, with a substantial body of evidence indicating that iMSCs can mediate immunosuppression through the secretion of factors such as TGF-β, IL-10, IL-6, and PTGS2[26,41–44] and further contribute to tumor angiogenesis and growth by secreting a variety of cytokines, such as vascular endothelial growth factor (VEGF), platelet-derived growth factor (PDGF), and fibroblast growth factor 2 (FGF2),[45–47] which represent potential risks that must be considered when utilizing iMSCs as therapeutic delivery vehicles for cancer treatment. However, numerous studies have confirmed that engineered iMSCs exhibit robust anti-tumor effects, with the benefits of delivering therapeutic factors outweighing the potential risks.[38,48–53] Based on our RNA-seq data, we observed that compared to B6-iMSCs, NKG2D-CAR-iMSCs exhibited a downregulation of immunosuppressive factors such as *IL-10*, *IL-6*, and *PTGS2* with only a slight upregulation of *TGF-β*. In contrast, pro-inflammatory cytokines such as *IL-33*, *IL-18*, and *IL-12* were significantly upregulated in NKG2D-CAR-iMSCs. This aligns with our *in vitro* co-culture results, which showed enhanced apoptosis of A549 cells, indicating that NKG2D-CAR engineering can further reduce the immunosuppressive risks associated with iMSCs. Additionally, angiogenesis-related factors such as *VEGF* and *PDGF* were also downregulated in NKG2D-CAR-iMSCs, suggesting a reduced risk of tumor angiogenesis promotion. Overall, the engineering of NKG2D-CAR enhances the tumor-targeting capabilities of iMSCs while further mitigating the risks of immunosuppression and tumor angiogenesis promotion.

It should be noted that the CAR structure utilized in this study was not specifically tailored for MSCs. The RNA-seq data indicate that the key enzymes required for the downstream signaling pathways of CD3ζ are expressed at very low levels in MSCs, suggesting that CD3ζ does not work in regulating the adhesion,

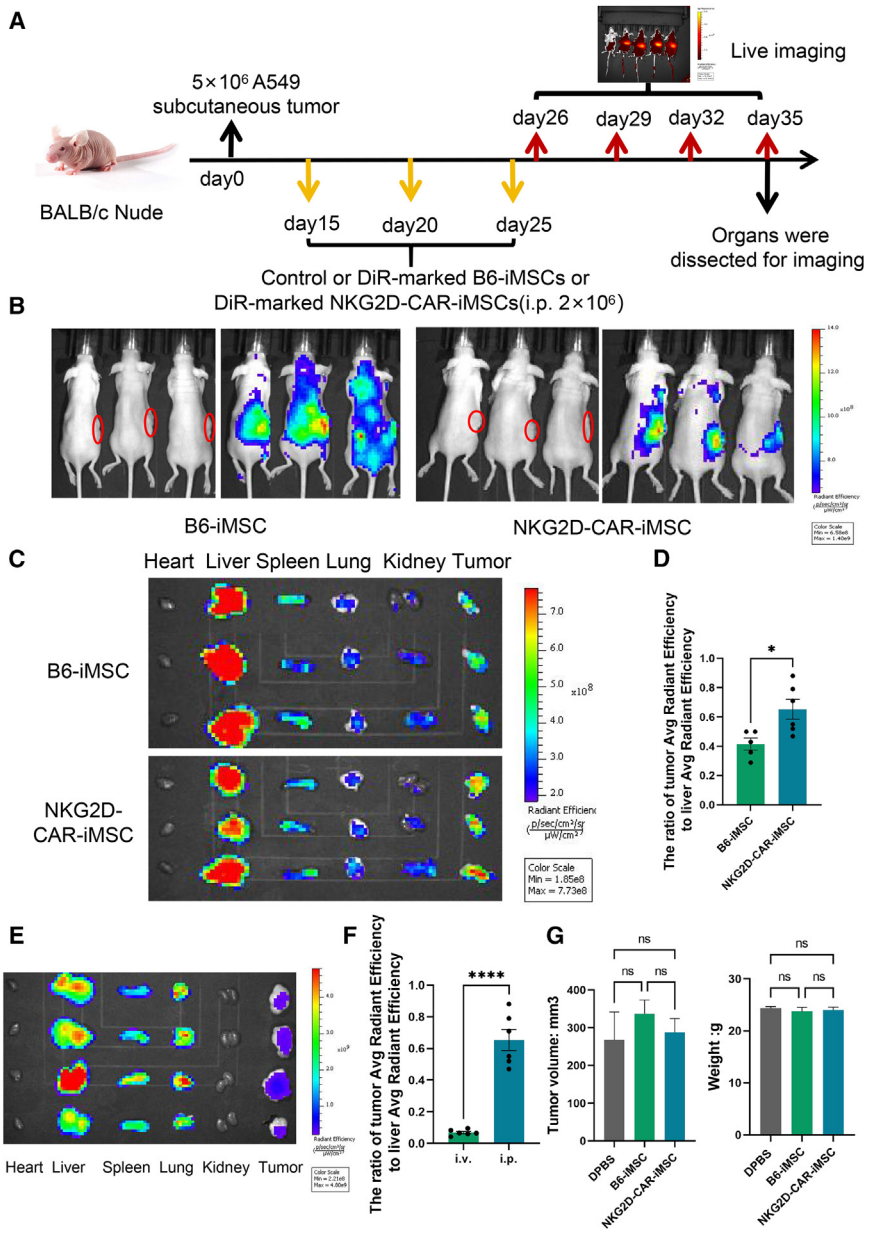

Figure 7. NKG2D-CAR improves iMSCs targeting and retention in the tumor in A549 xenograft model

(A) Schematic of animal experimental procedures.

(B) Live imaging of the dorsal side of mice three days post-iMSCs injection; red circle indicates tumor location.

(C) *Ex vivo* imaging of tumor tissues and mice organs.

(D) Ratio of tumor site signal to liver signal. (Data are mean ± SEM; n = 5–6; *p < 0.05, as determined by Student's two-tailed t test).

(E) *Ex vivo* imaging of tumor and mouse organs following intravenous (i.v.) injection.

(F) Ratio of tumor site signal to liver signal comparing i.v. and i.p. injections. (Data are mean ± SEM; n = 6; ****p < 0.0001, as determined by Student's two-tailed t test).

(G) Statistical analysis of tumor volume and mouse body weight, showing no significant differences (ns), as determined by one-way ANOVA.

migration, and immunomodulatory functions of MSCs that might introduce a limitation to our work.

In conclusion, our study demonstrates that NKG2D-CAR-iMSCs have an enhanced ability to target tumor cells expressing NKG2D-L in both *in vitro* and *in vivo* settings, opening new avenues for exploring iMSCs as a versatile, off-the-shelf carrier for the precise delivery of antitumor agents.

Limitations of the study

It should be noted that the CAR structure utilized in this study was not specifically tailored for MSCs, which might introduce a limitation to our work. Additionally, the animal model employed in this study was BALB/c nude mice, characterized by thymic hypoplasia, reduced T cell populations, and an incomplete immune system. These characteristics precluded an in-depth investigation of the TME and immune microenvironment, representing one of the principal limitations of this study.

RESOURCE AVAILABILITY

Lead contact

Further information and requests for resources and reagents should be directed to and will be fulfilled by the lead contact, Desheng Liang (liangdesheng@sklmg.edu.cn).

Materials availability

This study did not generate new, unique reagents.

Data and code availability

- RNA sequencing raw data generated in this study have been deposited to Sequence Read Archive (SRA: PRJNA1229859). These data are publicly available as of the date of publication. All data reported in this paper will be shared by the lead contact upon request.
- No original code was generated in this study.
- Any additional information required to reanalyze the data reported in this paper is available from the lead contact upon request.

ACKNOWLEDGMENTS

This work was funded by the National Natural Science Foundation of China (Grant Number 82271752) and the National Key Research and Development Program of China (2022YFC2703402 and 2022YFC2703604). The funders had no role in study design, data collection and analysis, decision to publish, or preparation of the manuscript. Graphical abstract was created in BioRender. Y.Z. (2025) https://BioRender.com/undefined.

AUTHOR CONTRIBUTIONS

Conceptualization, D.L.; methodology, Q.H. and S.T.; validation, S.T., Y.Z., Y.L., F.L., and M.H.; resources, D.L., F.L., M.H., and M.F.; data curation, Y.Z. and S.T.; writing—original draft preparation, S.T. and Y.Z.; writing—review and editing, D.L., P.W., Q.T., and M.Z.; visualization, S.T. and Y.Z.; funding acquisition, D.L. All authors have read and agreed to the published version of the manuscript.

DECLARATION OF INTERESTS

The authors declare no competing interests.

DECLARATION OF GENERATIVE AI AND AI-ASSISTED TECHNOLOGIES

During the preparation of this work, the authors used KiMi in order to polish the language. After using this tool, the authors reviewed and edited the content as needed and take full responsibility for the content of the publication.

STAR★METHODS

Detailed methods are provided in the online version of this paper and include the following:

- KEY RESOURCES TABLE
- EXPERIMENTAL MODEL AND STUDY PARTICIPANT DETAILS
  - Human iPSC line
  - Human PBMC
  - Animal
- METHOD DETAILS
  - Cell culture
  - Construction of B2M-NKG2D-CAR plasmid and transfection of iPSCs
  - Identification of site-specific integration NKG2D-CAR-iPSCs colonies
  - Karyotype analysis of iPSCs
  - Off-target detection
  - Quantitative real-time PCR
  - Generation and characterization of iPSC-derived iMSCs
  - MSC adherence ability detection
  - MSC migration assays in transwell system
  - RNA-sequencing and analysis
  - Animal experiments
  - Isolation and culturation of human PBMCs
  - Co-culture of iMSCs, PBMCs and tumor cells
  - Detection of immune cell activation, proliferation, and exhaustion
  - Detection of tumor cell apoptosis
- QUANTIFICATION AND STATISTICAL ANALYSIS

SUPPLEMENTAL INFORMATION

Supplemental information can be found online at https://doi.org/10.1016/j.isci.2025.112343.

Received: November 20, 2024
Revised: February 28, 2025
Accepted: March 31, 2025
Published: April 2, 2025

REFERENCES

1. Almeida-Porada, G., Atala, A.J., and Porada, C.D. (2020). Therapeutic mesenchymal stromal cells for immunotherapy and for gene and drug delivery. Mol. Ther. Methods Clin. Dev. *16*, 204–224. https://doi.org/10.1016/j.omtm.2020.01.005.
2. Khakoo, A.Y., Pati, S., Anderson, S.A., Reid, W., Elshal, M.F., Rovira, I.I., Nguyen, A.T., Malide, D., Combs, C.A., Hall, G., et al. (2006). Human mesenchymal stem cells exert potent antitumorigenic effects in a model of Kaposi's sarcoma. J. Exp. Med. *203*, 1235–1247. https://doi.org/10.1084/jem.20051921.
3. Bloor, A.J.C., Patel, A., Griffin, J.E., Gilleece, M.H., Radia, R., Yeung, D.T., Drier, D., Larson, L.S., Uenishi, G.I., Hei, D., et al. (2020). Production, safety and efficacy of iPSC-derived mesenchymal stromal cells in acute steroid-resistant graft versus host disease: a phase I, multicenter, open-label, dose-escalation study. Nat. Med. *26*, 1720–1725. https://doi.org/10.1038/s41591-020-1050-x.
4. Buitrago, J.C., Morris, S.L., Backhaus, A., Kaltenecker, G., Kaipa, J.M., Girard, C., Schneider, S., and Gruber, J. (2024). Unveiling the Immunomodulatory and regenerative potential of iPSC-derived mesenchymal stromal cells and their extracellular vesicles. Sci. Rep. *14*, 24098. https://doi.org/10.1038/s41598-024-75956-3.
5. De Becker, A., and Riet, I.V. (2016). Homing and migration of mesenchymal stromal cells: How to improve the efficacy of cell therapy? World J. Stem Cells *8*, 73–87. https://doi.org/10.4252/wjsc.v8.i3.73.
6. Dhar, P., and Wu, J.D. (2018). NKG2D and its ligands in cancer. Curr. Opin. Immunol. *51*, 55–61. https://doi.org/10.1016/j.coi.2018.02.004.
7. Duan, S., Guo, W., Xu, Z., He, Y., Liang, C., Mo, Y., Wang, Y., Xiong, F., Guo, C., Li, Y., et al. (2019). Natural killer group 2D receptor and its ligands in cancer immune escape. Mol. Cancer *18*, 29. https://doi.org/10.1186/s12943-019-0956-8.
8. Lazarova, M., and Steinle, A. (2019). The NKG2D axis: an emerging target in cancer immunotherapy. Expert Opin. Ther. Targets *23*, 281–294. https://doi.org/10.1080/14728222.2019.1580693.
9. Jones, A.B., Rocco, A., Lamb, L.S., Friedman, G.K., and Hjelmeland, A.B. (2022). Regulation of NKG2D Stress Ligands and Its Relevance in Cancer Progression. Cancers (Basel) *14*, 2339. https://doi.org/10.3390/cancers14092339.
10. Frazao, A., Rethacker, L., Messaoudene, M., Avril, M.-F., Toubert, A., Dulphy, N., and Caignard, A. (2019). NKG2D/NKG2-ligand pathway offers new opportunities in cancer treatment. Front. Immunol. *10*, 661. https://doi.org/10.3389/fimmu.2019.00661.
11. Yan, L., Li, J., and Zhang, C. (2023). The role of MSCs and CAR-MSCs in cellular immunotherapy. Cell Commun. Signal. *21*, 187. https://doi.org/10.1186/s12964-023-01191-4.
12. June, C.H., O'Connor, R.S., Kawalekar, O.U., Ghassemi, S., and Milone, M.C. (2018). CAR T cell immunotherapy for human cancer. Science *359*, 1361–1365. https://doi.org/10.1126/science.aar6711.
13. Chan, J.D., Lai, J., Slaney, C.Y., Kallies, A., Beavis, P.A., and Darcy, P.K. (2021). Cellular networks controlling T cell persistence in adoptive cell therapy. Nat. Rev. Immunol. *21*, 769–784. https://doi.org/10.1038/s41577-021-00539-6.

14. Hossian, A.K.M.N., Hackett, C.S., Brentjens, R.J., and Rafiq, S. (2022). Multipurposing CARs: Same engine, different vehicles. Mol. Ther. *30*, 1381–1395. https://doi.org/10.1016/j.ymthe.2022.02.012.

15. Golinelli, G., Grisendi, G., Prapa, M., Bestagno, M., Spano, C., Rossignoli, F., Bambi, F., Sardi, I., Cellini, M., Horwitz, E.M., et al. (2020). Targeting GD2-positive glioblastoma by chimeric antigen receptor empowered mesenchymal progenitors. Cancer Gene Ther. *27*, 558–570. https://doi.org/10.1038/s41417-018-0062-x.

16. Sirpilla, O., Sakemura, R.L., Hefazi, M., Huynh, T.N., Can, I., Girsch, J.H., Tapper, E.E., Cox, M.J., Schick, K.J., Manriquez-Roman, C., et al. (2024). Mesenchymal stromal cells with chimaeric antigen receptors for enhanced immunosuppression. Nat. Biomed. Eng. *8*, 443–460. https://doi.org/10.1038/s41551-024-01195-6.

17. Prakash, N., Kim, J., Jeon, J., Kim, S., Arai, Y., Bello, A.B., Park, H., and Lee, S.-H. (2023). Progress and emerging techniques for biomaterial-based derivation of mesenchymal stem cells (MSCs) from pluripotent stem cells (PSCs). Biomater. Res. *27*, 31. https://doi.org/10.1186/s40824-023-00371-0.

18. Zhou, H., He, Y., Xiong, W., Jing, S., Duan, X., Huang, Z., Nahal, G.S., Peng, Y., Li, M., Zhu, Y., and Ye, Q. (2023). MSC based gene delivery methods and strategies improve the therapeutic efficacy of neurological diseases. Bioact. Mater. *23*, 409–437. https://doi.org/10.1016/j.bioactmat.2022.11.007.

19. Zha, S., Tay, J.C.-K., Zhu, S., Li, Z., Du, Z., and Wang, S. (2020). Generation of Mesenchymal Stromal Cells with Low Immunogenicity from Human PBMC-Derived β2 Microglobulin Knockout Induced Pluripotent Stem Cells. Cell Transplant. *29*, 963689720965529. https://doi.org/10.1177/0963689720965529.

20. Hu, M., Zhang, Y., Liu, J., Chen, Y., Kang, J., Zhong, J., Lin, S., Liang, Y., Cen, R., Zhu, X., and Zhang, C. (2024). B2M or CIITA knockdown decreased the alloimmune response of dental pulp stem cells: an in vitro study. Stem Cell Res. Ther. *15*, 425. https://doi.org/10.1186/s13287-024-04023-5.

21. Han, A.R., Shin, H.R., Kwon, J., Lee, S.B., Lee, S.E., Kim, E.-Y., Kweon, J., Chang, E.-J., Kim, Y., and Kim, S.W. (2024). Highly efficient genome editing via CRISPR-Cas9 ribonucleoprotein (RNP) delivery in mesenchymal stem cells. BMB Rep. *57*, 60–65. https://doi.org/10.5483/BMBRep.2023-0113.

22. Zhou, M., Hu, Z., Qiu, L., Zhou, T., Feng, M., Hu, Q., Zeng, B., Li, Z., Sun, Q., Wu, Y., et al. (2018). Seamless Genetic Conversion of SMN2 to SMN1 via CRISPR/Cpf1 and Single-Stranded Oligodeoxynucleotides in Spinal Muscular Atrophy Patient-Specific Induced Pluripotent Stem Cells. Hum. Gene Ther. *29*, 1252–1263. https://doi.org/10.1089/hum.2017.255.

23. Sun, B., Yang, D., Dai, H., Liu, X., Jia, R., Cui, X., Li, W., Cai, C., Xu, J., and Zhao, X. (2019). Eradication of Hepatocellular Carcinoma by NKG2D-Based CAR-T Cells. Cancer Immunol. Res. *7*, 1813–1823. https://doi.org/10.1158/2326-6066.CIR-19-0026.

24. Feng, Z., Yang, Y., Liu, X.-Z., Sun, H.-J., Wen, B.-Y., Chen, Z., and Wei, B. (2025). Application of cell therapy in rheumatoid Arthritis: Focusing on the immunomodulatory strategies of Mesenchymal stem cells. Int. Immunopharmacol. *147*, 114017. https://doi.org/10.1016/j.intimp.2025.114017.

25. Ginting, A.R., Munir, D., Amin, M.M., Darlan, D.M., Putra, A., Rusda, M., Mutiara, E., Mayasari, E., and Rozi, M.F. (2024). Mesenchymal stem cells for immune modulation in systemic lupus erythematosus: From bench research to clinical applications. Narra J *4*, e994. https://doi.org/10.52225/narra.v4i3.994.

26. Aggarwal, S., and Pittenger, M.F. (2005). Human mesenchymal stem cells modulate allogeneic immune cell responses. Blood *105*, 1815–1822. https://doi.org/10.1182/blood-2004-04-1559.

27. Ng, J., Hynes, K., White, G., Sivanathan, K.N., Vandyke, K., Bartold, P.M., and Gronthos, S. (2016). Immunomodulatory Properties of Induced Pluripotent Stem Cell-Derived Mesenchymal Cells. J. Cell. Biochem. *117*, 2844–2853. https://doi.org/10.1002/jcb.25596.

28. Wang, P., Zhang, Y., Li, Z., Zhou, S., Tang, Q., Wang, Z., Xiao, R., Feng, M., Wu, L., and Liang, D. (2024). Mesenchymal Stem Cells Derived from Human Urine-Derived iPSCs Exhibit Low Immunogenicity and Reduced Immunomodulatory Profile. Int. J. Mol. Sci. *25*, 10394. https://doi.org/10.3390/ijms251910394.

29. Curio, S., Jonsson, G., and Marinović, S. (2021). A summary of current NKG2D-based CAR clinical trials. Immunother. Adv. *1*, ltab018. https://doi.org/10.1093/immadv/ltab018.

30. Gilham, D.E., Debets, R., Pule, M., Hawkins, R.E., and Abken, H. (2012). CAR-T cells and solid tumors: tuning T cells to challenge an inveterate foe. Trends Mol. Med. *18*, 377–384. https://doi.org/10.1016/j.molmed.2012.04.009.

31. Xie, G., Dong, H., Liang, Y., Ham, J.D., Rizwan, R., and Chen, J. (2020). CAR-NK cells: A promising cellular immunotherapy for cancer. EBioMedicine *59*, 102975. https://doi.org/10.1016/j.ebiom.2020.102975.

32. Liu, E., Marin, D., Banerjee, P., Macapinlac, H.A., Thompson, P., Basar, R., Nassif Kerbauy, L., Overman, B., Thall, P., Kaplan, M., et al. (2020). Use of CAR-Transduced Natural Killer Cells in CD19-Positive Lymphoid Tumors. N. Engl. J. Med. *382*, 545–553. https://doi.org/10.1056/NEJMoa1910607.

33. Dagher, O.K., and Posey, A.D. (2023). Forks in the road for CAR T and CAR NK cell cancer therapies. Nat. Immunol. *24*, 1994–2007. https://doi.org/10.1038/s41590-023-01659-y.

34. Labanieh, L., and Mackall, C.L. (2023). CAR immune cells: design principles, resistance and the next generation. Nature *614*, 635–648. https://doi.org/10.1038/s41586-023-05707-3.

35. Takayama, Y., Kusamori, K., Tsukimori, C., Shimizu, Y., Hayashi, M., Kiyama, I., Katsumi, H., Sakane, T., Yamamoto, A., and Nishikawa, M. (2021). Anticancer drug-loaded mesenchymal stem cells for targeted cancer therapy. J. Control. Release *329*, 1090–1101. https://doi.org/10.1016/j.jconrel.2020.10.037.

36. Leibacher, J., and Henschler, R. (2016). Biodistribution, migration and homing of systemically applied mesenchymal stem/stromal cells. Stem Cell Res. Ther. *7*, 7. https://doi.org/10.1186/s13287-015-0271-2.

37. Zhou, T., Yuan, Z., Weng, J., Pei, D., Du, X., He, C., and Lai, P. (2021). Challenges and advances in clinical applications of mesenchymal stromal cells. J. Hematol. Oncol. *14*, 24. https://doi.org/10.1186/s13045-021-01037-x.

38. Lan, T., Luo, M., and Wei, X. (2021). Mesenchymal stem/stromal cells in cancer therapy. J. Hematol. Oncol. *14*, 195. https://doi.org/10.1186/s13045-021-01208-w.

39. Golinelli, G., Grisendi, G., Dall'Ora, M., Casari, G., Spano, C., Talami, R., Banchelli, F., Prapa, M., Chiavelli, C., Rossignoli, F., et al. (2022). Anti-GD2 CAR MSCs against metastatic Ewing's sarcoma. Transl. Oncol. *15*, 101240. https://doi.org/10.1016/j.tranon.2021.101240.

40. Chiou, S.-H., Ong, H.K.A., Chou, S.-J., Aldoghachi, A.F., Loh, J.K., Verusingam, N.D., Yang, Y.-P., and Chien, Y. (2023). Chapter Five - Current trends and promising clinical utility of IPSC-derived MSC (iMSC). In Progress in Molecular Biology and Translational Science Stem Cell in Medicine, A. Higuchi, Y. Zhou, and S.-H. Chiou, eds. (Academic Press), pp. 131–154. https://doi.org/10.1016/bs.pmbts.2023.04.002.

41. Harrell, C.R., Volarevic, A., Djonov, V.G., Jovicic, N., and Volarevic, V. (2021). Mesenchymal Stem Cell: A Friend or Foe in Anti-Tumor Immunity. Int. J. Mol. Sci. *22*, 12429. https://doi.org/10.3390/ijms222212429.

42. Mathew, E., Brannon, A.L., Del Vecchio, A., Garcia, P.E., Penny, M.K., Kane, K.T., Vinta, A., Buckanovich, R.J., and di Magliano, M.P. (2016). Mesenchymal Stem Cells Promote Pancreatic Tumor Growth by Inducing Alternative Polarization of Macrophages. Neoplasia *18*, 142–151. https://doi.org/10.1016/j.neo.2016.01.005.

43. Ren, G., Zhang, L., Zhao, X., Xu, G., Zhang, Y., Roberts, A.I., Zhao, R.C., and Shi, Y. (2008). Mesenchymal stem cell-mediated immunosuppression occurs via concerted action of chemokines and nitric oxide. Cell Stem Cell *2*, 141–150. https://doi.org/10.1016/j.stem.2007.11.014.

44. Shi, Y., Hu, G., Su, J., Li, W., Chen, Q., Shou, P., Xu, C., Chen, X., Huang, Y., Zhu, Z., et al. (2010). Mesenchymal stem cells: a new strategy for immunosuppression and tissue repair. Cell Res. *20*, 510–518. https://doi.org/10.1038/cr.2010.44.

45. Shi, Y., Zhang, J., Li, Y., Feng, C., Shao, C., Shi, Y., and Fang, J. (2025). Engineered mesenchymal stem/stromal cells against cancer. Cell Death Dis. *16*, 113. https://doi.org/10.1038/s41419-025-07443-0.

46. Yu, W., Zhou, H., Feng, X., Liang, X., Wei, D., Xia, T., Yang, B., Yan, L., Zhao, X., and Liu, H. (2023). Mesenchymal stem cell secretome-loaded fibrin glue improves the healing of intestinal anastomosis. Front. Bioeng. Biotechnol. *11*, 1103709. https://doi.org/10.3389/fbioe.2023.1103709.

47. Niu, Q., He, J., Wu, M., Liu, J., Lu, X., Zhang, L., and Jin, Z. (2022). Transplantation of bone marrow mesenchymal stem cells and fibrin glue into extraction socket in maxilla promoted bone regeneration in osteoporosis rat. Life Sci. *290*, 119480. https://doi.org/10.1016/j.lfs.2021.119480.

48. Gao, P., Ding, Q., Wu, Z., Jiang, H., and Fang, Z. (2010). Therapeutic potential of human mesenchymal stem cells producing IL-12 in a mouse xenograft model of renal cell carcinoma. Cancer Lett. *290*, 157–166. https://doi.org/10.1016/j.canlet.2009.08.031.

49. Seo, S.H., Kim, K.S., Park, S.H., Suh, Y.S., Kim, S.J., Jeun, S.-S., and Sung, Y.C. (2011). The effects of mesenchymal stem cells injected via different routes on modified IL-12-mediated antitumor activity. Gene Ther. *18*, 488–495. https://doi.org/10.1038/gt.2010.170.

50. Wang, Z., Chen, H., Wang, P., Zhou, M., Li, G., Hu, Z., Hu, Q., Zhao, J., Liu, X., Wu, L., and Liang, D. (2022). Site-Specific Integration of TRAIL in iPSC-Derived Mesenchymal Stem Cells for Targeted Cancer Therapy. Stem Cells Transl. Med. *11*, 297–309. https://doi.org/10.1093/stcltm/szab031.

51. van Eekelen, M., Sasportas, L.S., Kasmieh, R., Yip, S., Figueiredo, J.-L., Louis, D.N., Weissleder, R., and Shah, K. (2010). Human stem cells expressing novel TSP-1 variant have anti-angiogenic effect on brain tumors. Oncogene *29*, 3185–3195. https://doi.org/10.1038/onc.2010.75.

52. Liu, B., Chen, F., Wu, Y., Wang, X., Feng, M., Li, Z., Zhou, M., Wang, Y., Wu, L., Liu, X., and Liang, D. (2017). Enhanced tumor growth inhibition by mesenchymal stem cells derived from iPSCs with targeted integration of interleukin24 into rDNA loci. Oncotarget *8*, 40791–40803. https://doi.org/10.18632/oncotarget.16584.

53. Studeny, M., Marini, F.C., Champlin, R.E., Zompetta, C., Fidler, I.J., and Andreeff, M. (2002). Bone marrow-derived mesenchymal stem cells as vehicles for interferon-beta delivery into tumors. Cancer Res. *62*, 3603–3608.

STAR★METHODS

KEY RESOURCES TABLE

REAGENT or RESOURCE	SOURCE	IDENTIFIER
Antibodies		
APC anti-human β2-microglobulin	Biolegend	Cat#316312; RRIDAB_10641281
PE anti-human HLA-A, B, C	Biolegend	Cat#311406; RRIDAB_314875
PE-Cy7 Mouse anti-human CD314(NKG2D)	BD Biosciences	Cat#562365; RRIDAB_11153309
anti-hULBP1 PE conjugated	R&D systems	Cat#FAB1380P; RRIDAB_2687471
anti-hULBP2/5/6 APC conjugated	R&D systems	Cat#FAB1298A; RRIDAB_2257142
x Human ULBP3	R&D systems	Cat#FAB1517R; RRIDAB_3646597
x Human MICA	R&D systems	Cat#FAB1300N; RRIDAB_3646264
x Human MICB	R&D systems	Cat#FAB1599T; RRIDAB_3646782
Brilliant Violet 421 anti-human CD34	Biolegend	Cat#343610; RRIDAB_2561358
Brilliant Violet 421 anti-human HLA-DR	Biolegend	Cat#307636; RRIDAB_2561831
Brilliant Violet 421 anti-human CD45	Biolegend	Cat#304032; RRIDAB_2561357
FITC anti-human CD44	Biolegend	Cat#338803; RRIDAB_1501204
PerCP/Cyanine5.5 anti-human CD73	Biolegend	Cat#344014; RRIDAB_2561757
APC anti-human CD105(Endoglin)	Biolegend	Cat#800508; RRIDAB_2687061
PE/Cyanine7 anti-human CD90(Thy1)	Biolegend	Cat#328124; RRIDAB_2561693
PE/Cyanine5 anti-human CD45	Biolegend	Cat#304010; RRIDAB_314398
Brilliant Violet 605 anti-human CD3	Biolegend	Cat#344836; RRIDAB_2565825
Alexa Flour 700 anti-human CD4	Biolegend	Cat#344622; RRIDAB_2563150
Brilliant Violet 570 anti-human CD8	Biolegend	Cat#301038; RRIDAB_2563213
PE anti-human CD25	Biolegend	Cat#356104; RRIDAB_2561861
PE/Cyanine7 anti-human CD69	Biolegend	Cat#310912; RRIDAB_314847
Brilliant Violet 421 anti-human FoxP3	Biolegend	Cat#320124; RRIDAB_2565972
Brilliant Violet 785 anti-human TIM-3	Biolegend	Cat#345032; RRIDAB_2565833
PE/Fire700 anti-human PD-1	Biolegend	Cat#621622; RRIDAB_2910489
APC/Cy7 anti-human CD107a	Biolegend	Cat#328630; RRIDAB_2562109
Brilliant Violet 750 anti-human IFN-γ	Biolegend	Cat#502550; RRIDAB_2832796
FITC anti-human GZMB	Biolegend	Cat#372206; RRIDAB_2687030
Brilliant Violet 650 anti-human Ki67	Biolegend	Cat#151215; RRIDAB_2876504
Alexa Flour 647 anti-human TCF7/TCF1	Biolegend	Cat#655203; RRIDAB_2566619
Brilliant Violet 510 anti-human CD56	Biolegend	Cat#318340; RRIDAB_2561944
Spark Blue 550 anti-human CD45RA	Biolegend	Cat#304185; RRIDAB_2941471
PE/Fire 810 anti-human CD197/CCR7	Biolegend	Cat#353269; RRIDAB_2894572
APC/Fire 810 anti-human CD95	Biolegend	Cat#305664; RRIDAB_2894542
ZOMBIE NIR	Biolegend	Cat#423105
Bacterial and virus strains		
DH5α Chemically Competent Cell	Tsingke	Cat#TSC-C14
Chemicals, peptides, and recombinant proteins		
Cell Trace FarRed Cell stain	Invitrogen	Cat#C34564A
Cell Trace Violet Cell stain	Invitrogen	Cat#C34557A
mTeSR Plus medium	STEMCELL Technologies	Cat#100–0276_C
Cas9 protein	Genscript	Cat#Z03702
1×DPBS	Gibco	Cat#C14190500BT
0.5 mM EDTA	Thermo Fisher Scientific	Cat#15575020

(*Continued on next page*)

Continued

REAGENT or RESOURCE	SOURCE	IDENTIFIER
Matrigel	BD Biosciences	Cat#354277
TrypLE Express	Gibco	Cat#12604-021
MEM-alpha basic medium	Gibco	Cat#8122725
Fetal bovine serum (FBS)	Sigma-Aldrich	Cat#F9423
XenoLight DiR	Revvity	Cat#125964
DMEM/high glucose medium	Gibco	Cat#C11995500BT
Glutamax	Gibco	Cat#35050061
Recombinant Human FGF basic/FGF2/bFGF Protein	R&D systems	Cat#3718-FB
Y-27632	STEMCELL Technologies	Cat#72304
2×Rapid Taq Master Mix	Vazyme	Cat#P222-03-AA
Colcemid	Sigma-Aldrich	Cat#C9754
Carnoy's fixative	Servicebio	Cat#G1120
2×Phanta Max Master Mix	Vazyme	Cat#P525-AA
TRIzol reagent	Invitrogen	Cat#15596018
HiScript II Q RT SuperMmix	Vazyme	Cat#R223-01
ChamQ Universal SYBR qPCR Master Mix	Vazyme	Cat#Q711-02
Dynabeads™ Human T-Activator CD3/CD28	Thermo Fisher	Cat#11131D
Recombinant Human Interleukin-2 for injection	SL PHARM	Cat#S19991007
RPMI 1640 medium	Gibco	Cat#11875093
Histopaque®-1077 sterile-filtered	Sigma-Aldrich	Cat#10771
ACK Lysis Buffer	Beyotime	Cat#C3702
Trypsin-EDTA (0.25%)	Thermo Fisher	Cat#25200056
Critical commercial assays		
STEMdiff Mesenchymal Progenitor Kit	STEMCELL Technologies	Cat#05240
FastPure Cell/Tissue DNA Isolation Mini Kit	Vazyme	Cat#DC102-01
PE Annexin V Apoptosis Detection Kit I	BD Pharmingen™	Cat#559763 RRID: AB2869265
eBioscience Foxp3/Transcription Factor Staining Buffer Set	Invitrogen	Cat# 00-5523-00
Deposited data		
RNA sequencing data	This paper	SRA: PRJNA1229859
Experimental models: Cell lines		
B6-iPSC (Zhou et al.[22])	This paper	N/A
A549	Procell	Cat#CL-0016
A375	Procell	Cat#CL-0014
H1299	Procell	Cat#CL-0165
H460	Procell	Cat#CL-0299
MCF7	Procell	Cat#CL-0149
Human PBMCs	This paper	N/A
Oligonucleotides		
sgRNA sequence: 5' -GGCCGAGATGTCTCGCTCCGTGG-3′	This paper	N/A
Primer: B2M-up-F/R and B2M-down-F/R, see Table S1	This paper	N/A
Primers for all the qPCR, see Table S1	This paper	N/A
Primers for off-target detection, see Table S1	This paper	N/A
Software and algorithms		
PerkinElmer *In Vivo* Imaging System	Perkin Elmer	N/A
GraphPad Prism 10	GraphPad Software	N/A
FlowJo	BD Bioscience	N/A

(*Continued on next page*)

Continued

REAGENT or RESOURCE	SOURCE	IDENTIFIER
Other		
PET Membrane Transwell Inserts	Corning	Cat#3464
Neon Transfection System	Invitrogen	Cat#MP927733
Bio-Rad CFX Manager software	Bio-Rad	N/A

EXPERIMENTAL MODEL AND STUDY PARTICIPANT DETAILS

Human iPSC line

A human iPSC cell line, which were reprogrammed from exfoliated renal tubular epithelial cells (urine cells) of a healthy male donor by our laboratory, named B6-iPSC,[22] was used in this study. Detailed information was reported in method details and key resources table.

Human PBMC

Human peripheral blood mononuclear cell (PBMC) isolated from a healthy 24-year-old female donor were utilized in this study. All experiments were conducted in accordance with the Declaration of Helsinki and approved by the Institutional Review Board of the School of Life Sciences, Central South University, Changsha, China. Informed consent was obtained from the female volunteer. Please check method details for detailed information of PBMC isolation and culturation.

Animal

Four-week-old male BALB/c nude mice were purchased from GemPharmatech Co., Ltd. (Nanjing, China). All animal experiments were approved by the Animal Ethics and Experimentation Committee of the School of Life Sciences, Central South University and all procedures were performed in accordance with relevant regulations. The protocol number of the research project approval documents is 2021-2-54.

METHOD DETAILS

Cell culture

We utilized mTeSR Plus medium (STEMCELL Technologies, Vancouver, BC, Canada, Cat#100–0276_C) for culturing iPSCs, which were reprogrammed from exfoliated renal tubular epithelial cells (urine cells) using episomes, as previously reported by our group. iPSCs reaching approximately 80% confluence were passaged with 0.5 mM EDTA (Thermo Fisher Scientific, Waltham, MA, USA, Cat#15575020), and plated onto fresh Matrigel-coated plates. (Matrigel, BD Biosciences, Bedford, MA, USA, Cat#354277). For the culturation of A549, A375, H1299, H460, MCF7 cells, which were purchased from Procell (Wuhan, China, Cat#CL-0016, Cat#CL-0014, Cat#CL-0165, Cat#CL-0299, Cat#CL-0149), we employed DMEM/high glucose (Gibco, Carlsbad, CA, USA, Cat#C11995500BT) supplemented with 10% fetal bovine serum (FBS) (Sigma-Aldrich, St. Louis, MO, US, Cat#F9423). iMSCs derived from iPSCs were cultured in α-MEM basic medium (Gibco, Cat#(8122725) supplemented with 10% FBS, 1% Glutamax (Gibco, Cat#35050061) and 10 μg/mL Recombinant Human FGF basic/FGF2/bFGF Protein (R&D systems, Minneapolis, MN, USA, Cat#3718-FB). All the cells mentioned above were cultured in disposable sterile dishes or flasks (Corning, NY, USA) in a humidified environment with 5% CO_2 at 37°C. Mycoplasma testing was performed and all human cell lines were authenticated using STR profiling within the past 3 years.

Construction of B2M-NKG2D-CAR plasmid and transfection of iPSCs

The B2M-NKG2D-CAR vector, which included B2M-NKG2D-CAR expression cassette and homology arms for targeting *B2M* exon1, were synthesized by Sangon Biotech (Shanghai, China). For gene targeting, we employed CRISPR/Cas9 system. Cas9 protein and sgRNA were purchased from Genescript (Genscript, Nanjing, China, Cat#Z03702), the sequence of sgRNA is as follows: 5' -GGCCGAGATGTCTCGCTCCGTGG-3'. Briefly, RNPs were formed by mixing 25 pmol Cas9 protein with 50 pmol of sgRNA in 20 μL of Buffer R (Invitrogen, Carlsbad, CA, USA, Cat#MPK10025B) and incubating at 37°C for 10 min iPSCs were dissociated with TrypLE-Express (Gibco, Cat 12604021) for 3 min until they became single cells and then counted. 1.5×10^6 cells were re-suspended in 100 μL of Buffer R containing 3 μg of the B2M-NKG2D-CAR vector and RNP. The Neon Transfection System (Invitrogen, Cat#MP927733) was used for completing nucleofection, with the transfection conditions set to voltage 1200 V, pulse width 20 ms and 2 pulses. The transfected cells were cultured in mTeSR Plus medium supplemented with 1/1000 Y-27632 (STEMCELL Technologies, Cat#72304). Seven days post-transfection, the integrated hiPSCs were dissociated into single cells and seeded into Matrigel-coated 6cm dishes to generate single colonies. Once colonies reached an appropriate size, they were picked artificially and transferred into Matrigel-coated 48-well plates for continued expansion culturation until they reached a sufficient cell quantity for further identification.

Identification of site-specific integration NKG2D-CAR-iPSCs colonies

Next, the iPSC colonies were identified using polymerase chain reaction, flow cytometry and quantitative real-time PCR. PCR was conducted using 2 × Rapid Taq Master Mix (Vazyme, Nanjing, China, Cat#P222-03-AA) according to the manufacturer's instructions after the iPSCs were lysate. Primer pairs, B2M-up-F/B2M-up-R, B2M-down-F/B2M-down-R, which share the same annealing temperature of 60°C, were used to identify the site-specific integration colonies. For flow cytometry, iPSCs were detached using TrypLE-Express, and after suspended at the concentration of 1 × 10^6 cells/mL, they were incubated with PE-Cy7-conjungated anti-human-CD314(NKG2D) (BD Bioscience, Cat#(562365) for 20 min. The stained cells were washed twice with 1 × DPBS (Gibco, Cat#C14190500BT). Flow cytometric analysis was performed using a Cytek Aurora flow cytometer and FlowJo software.

Karyotype analysis of iPSCs

B6-iPSCs and NKG2D-CAR-iPSCs were treated with 0.08 μg/mL colcemid (Sigma-Aldrich, Cat#C9754) for 2.5 h. Then, the cells were dissociated with 0.075 M KCL at 37°C for 30 min and fixed with Carnoy's fixative (a 3:1 mixture of methanol: acetic acid; Servicebio, China, Cat#G1120). Subsequently, metaphase chromosome spreads were prepared using standard procedures and air-dried. Giemsa trypsin banding staining was used to evaluate karyotyping.

Off-target detection

The potential off-target sites were predicted using an online tool (http://www.rgenome.net/cas-offinder/). The genomic DNA of B6-iPSCs and NKG2D-CAR-iPSCs were extracted using the FastPure Cell/Tissue DNA Isolation Mini Kit (Vazyme, Cat#DC102-01), which served as PCR templates. PCR was conducted using 2 × Phanta Max Master Mix (Vazyme, Cat#P525-AA) according to the manufacturer's instructions. Primer pairs—off-target-1-F/R, off-target-2-F/R, and off-target-3-F/R, whose sequences are shown in Table S1—were used to perform the PCR.

Quantitative real-time PCR

Total RNA was extracted using TRIzol reagent (Invitrogen, Cat#15596018), and RNA was converted into cDNA using an HiScript II Q RT SuperMix (Vazyme, Cat#R223-01). Quantitative PCR was performed according to the manufacturer's instructions, utilizing the ChamQ Universal SYBR qPCR Master Mix (Vazyme, Cat#Q711-02) on a Bio-Rad CFX96 Touch Real-Time PCR System (Bio-Rad, Hercules, CA, USA). Data analysis was conducted using Bio-Rad CFX Manager software (Bio-Rad). All primers used in this study are available in the database.

Generation and characterization of iPSC-derived iMSCs

We used the STEMdiff Mesenchymal Progenitor Kit (STEMCELL Technologies, Cat#05240) to differentiate iMSCs from iPSCs according to the manufacturer's protocol. Briefly, iPSCs were dispersed as single cells and cultured on Matrigel with mTeSR Plus medium until the confluence reached about 30%. Then, the medium was changed to STEMdiff -ACF mesenchymal induction medium. The STEMdiff-ACF mesenchymal induction medium was changed daily for the subsequent 4 days, and on day 5, the medium was changed to MesenCult-ACF Plus medium, which was continued through day 6. On day 7, cells were collected with TrypLE-Express and passaged onto a six-well plate precoated with the MesenCult-ACF attachment substrate. When the confluence reached 90%, cells were passaged onto a 6-cm dish pre-coated with MesenCult-ACF attachment substrate and cultured in MesenCult-ACF Plus medium until passage 5. The MesenCult-ACF medium was changed daily. Finally, MSC-like cells were seeded in 10-cm dishes pre-coated with gelatin and cultured in MSC medium. For the identification of the surface antigens expressed by iMSCs, the cells were firstly prepared at a concentration of 1 × 10^6 cells/mL in DPBS, then incubated with BV421-conjugated anti-human CD34/CD45/HLA-DR, BB515-conjugated anti-human CD44, PerCP-Cy5.5-conjugated anti-human CD73, APC-conjugated anti-human CD105, and PE-Cy7-conjugated anti-human CD90 (BD Biosciences), at room temperature for 20 min. Flow cytometric analysis was performed using a flow cytometer (BD Biosciences).

MSC adherence ability detection

The ability of iMSCs to adhere to tumor cells in different target-to-effector ratios was validated by flow cytometric analysis. Firstly, 4 × 10^5 iMSCs were stained with Cell Trace FarRed Cell stain (Invitrogen, Cat#C34564A) then cultured in twelve-well plates. 12 h later, 2 × 10^5, 4 × 10^5 or 8 × 10^5 tumor cells (A549, H460, H1299, MCF7) labeled with Cell Trace Violet Cell stain (Invitrogen, Cat#C34557A) were add to the wells. After 1.5 h co-culture, cells were dissociated with TrypLE Express. Finally, flow cytometric analysis was performed to estimate the percentage of double-positive cells.

MSC migration assays in transwell system

We used PET Membrane Transwell Inserts (Corning, 8.0-μm pores, 24-well plate) to perform the MSC migration assays. The iMSCs were treated with α-MEM basic medium (Gibco, Cat#(8122725) without FBS in advance. 12 h later, 2 × 10^4 iMSCs labeled with Cell Trace Far-Red stain in 150 μL α-MEM basic medium were added to the upper chambers, and 6 × 10^4 tumor cells (A549, A375, H1299, MCF7) in 800 μL α-MEM containing 10% FBS was added to the lower chambers. After coculturing for 36 h, we collected all cells from the lower chamber to analyze the percentage of FarRed positive cells by flow cytometry. Tumor cells cultured alone served as a negative control.

RNA-sequencing and analysis

RNA sequencing was performed at Shanghai Majorbio Bio-pharm Biotechnology Co., Ltd. (Shanghai, China). Our bioinformatic data were analyzed on the Majorbio Cloud Platform (Majorbio Bio-pharm Biotechnology, China). DESeq2 (http://bioconductor.org/packages/stats/bioc/DESeq2/) was used for gene differential expression analysis, the default screening criteria for significantly differentially expressed genes set to adjusted p-value <0.05 & $|\log2FC| \geq 1$. Perseus v.1.6.1.1 (http://www.coxdocs.org/doku.php?id=perseus:start) was used to generate heat maps and perform hierarchical clustering, while Goatools (https://github.com/tanghaibao/GOatools) was utilized for GO enrichment analysis. The raw data has been uploaded to NCBI and the BioProject number is PRJNA1229859.

Animal experiments

This study was approved by the Animal Ethics and Experimentation Committee of the School of Life Sciences, Central South University. Four-week-old BALB/c nude mice were purchased from GemPharmatech Co., Ltd. (Nanjing, China). Mice were injected subcutaneously in the right flank with 5×10^6 A549 cells for tumor implantation. When the tumor volume grew to about 200 mm^3, 2×10^6 iMSCs labeled with XenoLight DiR (Revvity, MA, USA, Cat#(125964) were injected once every five days for a total of three injections. The distribution of the iMSCs was then assessed every 3 days using the PerkinElmer *In Vivo* Imaging System (PerkinElmer, MA, USA). At the experimental endpoint, peripheral blood of the mice was collected from the submandibular venous plexus of the mice, which were then euthanized by cervical dislocation and subsequently dissected, followed by imaging of the heart, liver, spleen, lungs, kidneys, and tumors using the PerkinElmer *In Vivo* Imaging System (PerkinElmer, MA, USA). The peripheral blood was allowed to stand at room temperature for 2 h. After that, it was centrifuged at 3000 rpm for 15 min, the upper layer plasma was collected and sent to Servicebio (China) for liver and renal function analytical biochemical tests. The weight of the mice and the dimensions of the tumor sizes (including length and width) were measured at regular intervals. The tumor volumes were calculated according to the following formula: tumor volume (mm^3) = length × width × 0.52.

Isolation and culturation of human PBMCs

Freshly collected peripheral blood was collected and then diluted by an equal volume of 1 × DPBS, then Histopaque-1077 sterile-filtered (Sigma-Aldrich, Cat#10771) was utilized to separate PBMCs follow the standard instructions. After washed by 1× DPBS twice, the PBMCs were resuspended with 3mL ACK Lysis Buffer (Beyotime Biotechnology, Cat#C3702) and incubation at room temperature for 10 min for red blood cell lysis. After terminating the lysis by adding 4 mL RPMI 1640 medium (Gibco, Cat#11875093) into the cell suspension and centrifugating at 300×g for 5 min, the PBMCs were resuspended with 10 mL RPMI 1640 mediumand seeded into a 10 cm dish. 24 h later, we counted the cells and added Dynabeads Human T-Activator CD3/CD28 (Thermo Fisher Scientific, Cat#11131D) to the cell culturation at a cell-to-bead ratio of 10:1, and Recombinant Human Interleukin-2 (SL PHARM, Cat#S19991007) was supplemented to a final concentration of 100 IU/mL for activation. The PBMCs were activated for in disposable sterile dishes or flasks in a humidified environment with 5% CO_2 at 37°C for 72 h and then used for subsequent co-culture experiments.

Co-culture of iMSCs, PBMCs and tumor cells

The tumor cells were labeled with Cell Trace Violet Cell Stain follow the instructions and co-cultured with iMSCs at an effector-to-target ratio of 1:5 in a 6-well plate (3×10^5 iMSCs per well and 6×10^4 tumor cells per well). After 12 h, when the iMSCs and tumor cells had adhered to the plate, 6×10^5 PBMCs, which beads and IL-2 was removed 24 h in advance, were added to the co-culture system. After 48 h of co-culture, the apoptosis rate of tumor cells and the proliferation, activation, and exhaustion of immune cells were assessed through flow cytometry.

Detection of immune cell activation, proliferation, and exhaustion

PBMCs were collected from the co-culture system and centrifuge at 300×g for 5 min at room temperature and washed once with 1 × DPBS. Stain the PBMCs with the antibodies PE/Cyanine5 anti-human CD45, Brilliant Violet 605 anti-human CD3, Alexa Fluor 700 anti-human CD4, Brilliant Violet 570 anti-human CD8, PE anti-human CD25, PE/Cyanine7 anti-human CD69, APC/Cy7 anti-human CD107a, Brilliant Violet 510 anti-human CD56, Spark Blue 550 anti-human CD45RA, PE/Fire 810 anti-human CD197/CCR7, APC/Fire 810 anti-human CD95, PE/Fire700 anti-human PD-1, Brilliant Violet 785 anti-human TIM-3 (Biolegend, Cat#304010, Cat#344836, Cat#344622, Cat#301038, Cat#356104, Cat#310912, Cat#328630, Cat#318340, Cat#304186, Cat#353269, Cat#305664, Cat#621622, Cat#345032) for 20–30 min according to the manufacturer's instructions. After staining, wash the cells once with 1× DPBS. Use the eBioscience FOXP3/Transcription Factor Staining Buffer Set (Invitrogen, Cat#00-5523-00) to permeabilize the cells for 1 h following the standard protocol, then stain the cells with antibodies Brilliant Violet 421 anti-human FoxP3, Brilliant Violet 750 anti-human IFN-γ, FITC anti-human GZMB, Brilliant Violet 650 anti-human Ki67, Alexa Fluor 647 anti-human TCF7/TCF1(Biolegend, Cat#320124, Cat#502550, Cat#372206, Cat#151215, Cat#355204) for 20–30 min in 100 μL 1 × permeabilization buffer. After washed once with 1 mL 1 × permeabilization buffer the cells were resuspended in 300 μL 1 × permeabilization buffer and analyzed using a flow cytometer.

Detection of tumor cell apoptosis

Digest and collect the co-cultured cells using TrypLE-Express. After centrifuging the cells at 175 g for 5 min at room temperature and wash once with 500 μL 1 × DPBS, we utilized the BD Pharmingen PE Annexin V Apoptosis Detection Kit I (BD Pharmingen, Cat#559763, RRID: AB2869265) to detect apoptosis. Specifically, resuspend the cells in 100 μL of 1 × Binding Buffer, add 5 μL of PE-Annexin V and 5 μL of 7-AAD stain, and incubate in the dark at room temperature for 15 min. Finally resuspended the cells with 300 μL1 × Binding Buffer and analyze the apoptosis of tumor cells using a flow cytometer.

QUANTIFICATION AND STATISTICAL ANALYSIS

Prism8 (GraphPad Software) was utilized to analyze all statistics generated from this study. As indicated in the figure legends, for comparing the two experimental groups with normally distributed data, an unpaired two-tailed Student's t test was employed. Two-way analysis of variance (ANOVA) followed by Dunett's multiple comparison test or one-way ANOVA was used to compare the various experimental groups. The data were presented as mean ± SEM, and $p < 0.05$ was considered statistically significant. Detailed information are as follows. Figure 1D, Student's two-tailed *t*-test, $n = 3$ ***$p < 0.001$; Figure 2D, Student's two-tailed t-test, $n = 3$ ****$p < 0.0001$; Figure 3C, one-way ANOVA, *$p < 0.05$, **$p < 0$ 0.01, ***$p < 0.001$, ****$p < 0.0001$; Figure 4C, Student's two-tailed *t*-test, *$p < 0.05$, **$p < 0$ 0.01, ****$p < 0.0001$; Figure 5E, Student's two-tailed *t*-test, *$p < 0.05$, **$p < 0$ 0.01, ***$p < 0.001$, ****$p < 0.0001$; Figures 6B and 6D–6H, one-way ANOVA, *$p < 0.05$, **$p < 0$ 0.01, ***$p < 0.001$, ****$p < 0.0001$; Figure 7D, Student's two-tailed *t*-test, *$p < 0.05$; Figure 7F, Student's two-tailed *t*-test, ****$p < 0.0001$; Figure 7G, one-way ANOVA.